ARL-TR-9434 ● MAY 2022

DEVCOM ARMY RESEARCH LABORATORY

Hierarchical Diamond-Based Ceramic Composites (Summary Technical Report, Oct 2019 – Sep 2021)

by Anthony DiGiovanni, Shawn Coleman, Matthew Guziewski, Jerry LaSalvia, Jennifer Dunn, Mathew Ivill, S Vennila Raju, Michael Kornecki, Samuel G Hirsch, William T Shoulders, Raymond Brennan, Scott Walck, Philip Goins, Thomas Scharf, Brian Schuster, Jonathan Ligda, Daniel Magagnosc, Brian Powers, Richard B Leavy, John Clayton, and Debjoy Mallick

Approved for public release: distribution unlimited.

NOTICES

Disclaimers

The findings in this report are not to be construed as an official Department of the Army position unless so designated by other authorized documents.

Citation of manufacturer's or trade names does not constitute an official endorsement or approval of the use thereof.

Destroy this report when it is no longer needed. Do not return it to the originator.

ARL-TR-9434 ● MAY 2022

Hierarchical Diamond-Based Ceramic Composites (Summary Technical Report, Oct 2019 – Sep 2021)

Anthony DiGiovanni, Shawn Coleman, Matthew Guziewski, Jerry LaSalvia, Mathew Ivill, Samuel G Hirsch, William T Shoulders, Raymond Brennan, Philip Goins, Thomas Scharf, Jonathan Ligda, Daniel Magagnosc, Brian Powers, Richard B Leavy, John Clayton, Debjoy Mallick, and Jennifer Dunn
DEVCOM Army Research Laboratory

S Vennila Raju, Michael Kornecki, and Scott Walck
SURVICE Engineering

Brian Schuster
University of Texas at El Paso

Approved for public release: distribution unlimited.

REPORT DOCUMENTATION PAGE

Form Approved
OMB No. 0704-0188

Public reporting burden for this collection of information is estimated to average 1 hour per response, including the time for reviewing instructions, searching existing data sources, gathering and maintaining the data needed, and completing and reviewing the collection information. Send comments regarding this burden estimate or any other aspect of this collection of information, including suggestions for reducing the burden, to Department of Defense, Washington Headquarters Services, Directorate for Information Operations and Reports (0704-0188), 1215 Jefferson Davis Highway, Suite 1204, Arlington, VA 22202-4302. Respondents should be aware that notwithstanding any other provision of law, no person shall be subject to any penalty for failing to comply with a collection of information if it does not display a currently valid OMB control number.
PLEASE DO NOT RETURN YOUR FORM TO THE ABOVE ADDRESS.

1. REPORT DATE *(DD-MM-YYYY)*	2. REPORT TYPE	3. DATES COVERED (From - To)
May 2022	Summary Technical Report	1 October 2019–30 September 2021

4. TITLE AND SUBTITLE
Hierarchical Diamond-Based Ceramic Composites (Summary Technical Report, Oct 2019 – Sep 2021)

5a. CONTRACT NUMBER

5b. GRANT NUMBER

5c. PROGRAM ELEMENT NUMBER

6. AUTHOR(S)
Anthony DiGiovanni, Shawn Coleman, Matthew Guziewski, Jerry LaSalvia, Jennifer Dunn, Mathew Ivill, S Vennila Raju, Michael Kornecki, Samuel G Hirsch, William T Shoulders, Raymond Brennan, Scott Walck, Philip Goins, Thomas Scharf, Brian Schuster, Jonathan Ligda, Daniel Magagnosc, Brian Powers, Richard B Leavy, John Clayton, and Debjoy Mallick

5d. PROJECT NUMBER
611102.AA7.03

5e. TASK NUMBER

5f. WORK UNIT NUMBER

7. PERFORMING ORGANIZATION NAME(S) AND ADDRESS(ES)
DEVCOM Army Research Laboratory
ATTN: FCDD-RLW-ME
Aberdeen Proving Ground, MD 21005

8. PERFORMING ORGANIZATION REPORT NUMBER
ARL-TR-9434

9. SPONSORING/MONITORING AGENCY NAME(S) AND ADDRESS(ES)

10. SPONSOR/MONITOR'S ACRONYM(S)

11. SPONSOR/MONITOR'S REPORT NUMBER(S)

12. DISTRIBUTION/AVAILABILITY STATEMENT
Approved for public release: distribution unlimited.

13. SUPPLEMENTARY NOTES
ORCID IDs: Anthony DiGiovanni, 0000-0003-3344-1753; John Clayton, 0000-0003-4107-6282; Shawn Coleman, 0000-0002-5542-3161; Matthew Guziewski, 0000-0002-5761-720X; Richard Leavy, 0000-0002-7243-1198; Jonathan Ligda, 0000-0003-3539-8867; Daniel Magagnosc, 0000-0002-1418-9292

14. ABSTRACT
A basic science 6.1 research program was undertaken in hierarchically designed diamond–silicon carbide (SiC) composites in support of the Army Modernization Priorities in Soldier Lethality. An innovative combination of experimental synthesis and testing and multiscale simulation techniques explored the effects of hierarchical microstructure (mesoscale diamond packing and nanoscale interfaces) on the mechanical and ballistic performance of these composite ceramics. Critical relationships at the mesoscale were identified, allowing predictive deformation by integrating microstructural characterization with experimental microcantilever failure and atomistically informed grain boundary energies. Diamond-SiC and SiC-SiC interfaces played a crucial role in the fracture toughness and compressive strength of the diamond composites, and controlling these interfaces may eventually be used to manipulate the failure mechanisms that improve ballistic performance. The developed approach allows for the analysis of not just pristine interfaces, but interfaces that more closely resemble those seen experimentally. Additionally, this study created an interactive loop linking fundamental powder-based processing variables to Monte Carlo Potts simulations and evolved microstructures that can be evaluated in mesoscale phase field models.

15. SUBJECT TERMS
STR, silicon carbide, diamond, ICME, integrated computational materials engineering, phase field modeling, Monte Carlo Potts modeling, LAMMPS molecular dynamics, density functional theory, reaction-bonded composites, spark plasma sintering, percolation theory, particle packing, Sciences of Extreme Materials

16. SECURITY CLASSIFICATION OF:			17. LIMITATION OF ABSTRACT	18. NUMBER OF PAGES	19a. NAME OF RESPONSIBLE PERSON
a. REPORT	b. ABSTRACT	c. THIS PAGE			Anthony DiGiovanni
Unclassified	Unclassified	Unclassified	UU	66	19b. TELEPHONE NUMBER (Include area code) (410) 306-4587

Standard Form 298 (Rev. 8/98)
Prescribed by ANSI Std. Z39.18

Contents

List of Figures

List of Tables

Executive Summary

The enclosed record is a summary technical report on technology innovation and advancement completed by the US Army Combat Capabilities Development Command Army Research Laboratory and collaborators from October 2019 to September 2021, under 611102.AA7.03 Emerging Materials Research. This 6.1 research program into hierarchically designed diamond ceramic composites uncovered critical relationships in the mesoscale response of diamond-silicon carbide by linking the experimentally observed grain-scale deformations with atomistically informed grain boundary energy that enabled a predictive understanding of failure. Moreover, this study for the first time created an interactive modeling loop linking fundamental powder-based processing variables to sintered microstructures that could be related to mesoscale phase field inputs and outputs. This foundational work established the basis for continuing efforts in new material systems explored in follow-on research to support the Army mission.

1. Program Objectives

This research developed and utilized advanced processing, modeling, and micromechanical tools to discover and demonstrate hierarchically structured diamond-based composites with exceptional mechanical and ballistic behavior. Understanding how nanoscale and mesoscale microstructural features in diamond–silicon carbide (SiC) composites influenced the physics of failure was critical in uncovering ways to improve performance for Soldier protection and discover potential defeat mechanisms. Emphasis was placed on the fundamental understanding of the deformation and failure mechanisms, which enabled the design and development of robust materials to support Army core functions. Development of new materials was the focus of this study with specific emphasis on fundamental knowledge of microstructural grain boundaries in diamond-SiC composites. Novel processing routes to selectively tailor the nano-mesoscale microstructure in heterogeneous ceramic armors were explored via conventional hot-pressing, reactive hot-pressing, and spark plasma sintering (SPS). Correlations between the nano-mesoscale hierarchical microstructure, deformation mechanisms, and mechanical response were explored using advanced characterization methods and small-scale mechanical testing. Higher fidelity mesoscale mechanics models were sought by using experimentally obtained microstructural information coupled with atomistic models of relevant grain boundary interfaces. In turn, the mesoscale model outputs guided experiments for achieving optimal nano-mesoscale hierarchical microstructures and inform continuum ballistic models.

2. Current State of the Art

SiC and boron carbide (B_4C) have long been investigated as materials critical to the performance of armor ceramic and related systems.[1] Their combination of high hardness, low density, and strength have long been identified among the key differentiating characteristics for ceramic materials.[2,3] Over roughly the last two decades, diamond-SiC composites have been developed for commercial applications requiring high abrasion resistance, thermal stability, and thermal conductivity.[4,5] Thus, it follows that composites made from the hardest known bulk material, diamond, could be integrated and optimized for armor ceramic systems, a leap forward in ballistic performance may be feasible.

Commercial applications have been realized without need for extensive understanding of their mechanical deformation or physics of failure under extremely high strain rates and stress states found in ballistic impact. Emergence of advanced kinetic energy threats have increased demand for game-changing armor

solutions for Soldier protection. While extensive work at the US Army Combat Capabilities Development Command (DEVCOM) Army Research Laboratory (ARL) has improved the knowledge and performance of SiC- and B_4C-based armors, the inclusion of diamond has received comparatively little attention. Globally, the diamond grit industry is driving down costs such that diamond-based composite armor solutions are more tractable.

These factors combined to inspire this basic research study in diamond-based ceramic composites to understand the relationships between processing methods, parameters, and resultant hierarchical microstructure on the mechanical and ballistic performance.

The most common low-pressure processing route is a liquid silicon (Si) infiltration method[6–8] where Si reacts with a carbon (C) source to form SiC under ambient or low pressure. Diamond-SiC composites made by this technique[9–11] require a minimum of large open pathways between the diamond particulates for Si migration, which constrains the amount of diamond solids loading. Low C diffusivity in SiC can also limit the reaction leaving residual Si metal within the matrix if the initial distribution of carbon and infiltration pathways are not carefully optimized.

Research studies investigating diamond ceramic composites currently produced using these methods have shown that their performance is linked to hierarchical microstructure features. In diamond-SiC these hierarchical microstructural features can be divided between the mesoscale distribution of super hard diamond particulates and the nanoscale interfaces between the diamond-SiC and SiC grain boundaries. The prior research studies have shown there are likely correlations between these hierarchical features on the mechanical response. For example, the overall concentration of diamond particulates plays a major role in the hardness as described by composite theory.

Prior work in this area noted that the performance of diamond-SiC is also influenced strongly by the interfacial strength between diamond and SiC[12] and that decreasing the grain size of the SiC matrix can improve the fracture toughness from 8 to 12 $MPa \cdot m^{1/2}$ (a dramatic increase over bulk diamond at 3–5 $MPa \cdot m^{1/2}$).[13] Because the initial intended application of these composites were never for armor, prior research on the terminal mechanics of diamond-SiC under high strain rates is extremely limited. The only known ballistic data on high-solids content diamond materials was collected by Lundberg et al.[14], which demonstrated a 45% improvement over B_4C in the transition impact velocity against tungsten heavy alloy penetrators. Extensive studies have not examined the ballistic response of polycrystalline or single crystalline diamond due to high material costs and

unavailability in sizes of interest (or unavailability in subscale ballistic testing methodologies with time-history diagnostic capabilities).

3. Research Efforts

This effort was pursued through the following four key thrust areas:

3.1 Processing

Processing techniques investigated methods to control the hierarchical microstructural features of diamond-SiC composites at the mesoscale (packing of diamond) and nanoscale (interfaces between diamond-SiC and SiC grain boundaries) using novel and conventional processing methods. To achieve desired microstructures, this program examined lower-temperature (1450–1600 °C) reaction bonding processes using powder-based formulations, instead of traditional melt infiltration techniques. Special processing methods for generating bilayers, laminates, and graded-layer composites were also studied to explore interface engineering more systematically as well as understand the effects residual stress-states on the mechanical and ballistic performance.

3.1.1 Monolithic Diamond-SiC Hierarchical Microstructures

A multimodal powder-based, low-temperature, high-diamond content process was achieved by careful selection of coarse, medium, and fine particle size distributions of the constitutive phases. Using conventional hot-pressing, the limits of diamond additions will be explored and explained by percolation theory. Alternate synthesis approaches used a mixture of key phases such as diamond, non-diamond carbon, SiC and ultimately silicon powder to react and densify the structure in place. Moderate pressure assisted the Si metal infiltration and reduced diamond intergranular interstices. Assuming adequate premixing, the Si-C reaction cements the diamond phase in place without reliance on extensive C diffusion. Further exploration of the reactive powder synthesis was examined by traditional spark plasma sintering (SPS). All processes were implemented in an inert environment (vacuum or Ar gas) and at temperatures below the point where severe diamond degradation occurs (~1600 °C). Diamond-SiC composites were created or obtained with varying diamond-particle loading from 40 vol% up to this maximum (~70 vol%) by using different particle size distributions.

Prior work has shown that an amorphous C nanolayer is common at the diamond-SiC interface in these composites. The presence and thickness of this amorphous film can switch the prominent fracture mode from transgranular to intergranular. Understanding the development of the non-diamond carbon grain boundary phase

will be critical to controlling bulk performance. Mesoscale fracture toughness may be modified if the boundary phase is controlled and ultimately lead to improve ballistic response, even at the expense of reduced hardness.

3.1.2 Diamond-SiC and SiC-SiC Bilayers

Bilayer structures were created to understand the nanoscale processing-structure-property relationship in more detail without geometrical constraints caused by powder packing. Bilayers were produced from single crystal synthetic diamond and SiC wafers by heat treating in a hot-press with a low applied pressure and relatively low temperature (near processing temperatures). Here, additives can be selectively deposited to alter the chemistry of the interfaces and determine their effects on small-scale mechanical strength. Additional heat treating can be done to examine its effects on the thickness of the amorphous C nanolayer film and SiC grain boundary complexion stability and interfacial tensile strengths (i.e., microcantilever beam experiments).

3.2 Microstructural and Mechanical Characterization

Advanced characterization methods were used to identify structure-property relationships within the diamond-SiC composites. X-ray diffraction (XRD) and Raman spectroscopy was employed to quantify both bulk and local residual stress levels in the composites and layered structures. Analytical electron microscopy (AEM) techniques were implemented to further quantify the stress states that originate from nanoscale microstructural features, such as interfaces. These methods were used to determine the thickness of amorphous C films expected at the interfaces and understand interface structures predicted by atomistic simulations by comparing observed structures to the optimized models.

Microstructural knowledge of the interface network is necessary to understand the fracture behavior of the diamond-SiC composite. Scanning electron microscopy (SEM) and electron backscatter diffraction (EBSD) obtained 2D microstructures of the phase distribution and SiC grain boundary structure. Focused ion beam (FIB) and femtosecond laser (FSL) coupled tomography was employed to create volumes large enough to observe both the diamond and SiC phases. The 2D and 3D microstructure data were used as real-world input for mesoscale mechanics-based models. Smaller volumes focused specifically on the diamond-SiC interfaces were sampled using higher resolution and reduced size scale of the FIB.

Microcantilever beam and microcompression tests were used to focus on both singular diamond-SiC interfaces and small aggregates. To understand better the influence that the interface networks, a range of sample sizes was explored

containing a varying amount and type of interfaces. The collective behavior of large interface networks was studied using FSL-based microtension tests, which enabled rapid population of statistically significant failure distributions. A micropillar-based method designed to drive preferential growth along boundaries was conducted to supplement these traditional methods. Other small-scale testing methods was conducted to determine the influence of interfaces and grain boundaries on the mechanical response.

3.3 Multiscale Modeling

Multiscale models provided predictive capabilities showing how processing conditions can be tuned to achieve hierarchical microstructural features in diamond-SiC composites and how mesoscale mechanical responses are affected by the underlying interfaces and grain boundaries. A high-throughput atomistic study on the interface energetics and mechanical properties served as the basis for parameterization of these mesoscale models. Atomistic structures will be validated through comparisons with experimental scanning transmission electron microscopy (STEM) as well as performance trends observed in microcantilever beam studies. Similarly, mesoscale models will be validated through comparisons with experimental 3D microstructure, micropillar mechanical tests, and subscale ballistics experiments.

3.3.1 Atomistic Models of Interface Structure Properties

The high-throughput atomic models in support of mesoscale efforts were constructed for the diamond-SiC interface as well as diamond and SiC grain boundaries. For the SiC and diamond homophase systems, interatomic potentials exist but need to be further evaluated for the grain boundary structures to reasonably capture the energy and force landscape for these individual components. Interatomic potentials were evaluated for the diamond-SiC heterophase system; however, it is expected that more accurate composite interface models will require quantum-based simulations. Atomistic models explored the 10 degrees of freedom (DOF) that are needed to describe the diamond-SiC interface and grain boundaries (5 DOF for grain orientations, 3 DOF for local microstructure relaxation, and 2 DOF for grain phase). Additionally, atomistic models explored the formation of the amorphous intergranular films observed to effect microstructure evolution and mechanics. The high-throughput atomistic study computed interfacial energetics (minimum energy and nonequilibrium structures), as well as systematically modeled the interface elastic and plastic mechanical response. While elastic response was largely expected to follow mixing rules for composite materials, the interface structure was expected to play a role in the overall plastic response and

failure. Data about the model parameters and calculation results were stored using the National Institute of Standards and Technology (NIST) Materials Data Curation system to better enable analytics for parameterizing to mesoscale models and capturing uncertainty.

3.3.2 Mesoscale Models of Grain Growth and Mechanics

Data from the atomic simulations helped parameterize mesoscale grain growth and mechanics-based models. First, surrogate models were developed that recast the energetic and mechanical responses computed by the high-throughput atomistic study into reduced ordered functions that were more easily incorporated into mesoscale models. Principal component analysis, applied to the atomistic results, reduced the many DOF explored in the high-throughput study. Hierarchical microstructure evolution in diamond-SiC was modeled using mesoscale grain growth models parameterized by the interface energetic data from atomistic simulations as well as experiments. To model the microstructure evolution occurring during the reaction bonding process, 3D kinetic Monte Carlo Potts (MCP) grain growth models studied the effects of large diamond particles on the SiC matrix grain growth.

Continuum mesoscale models were used to evaluate the local response and overall failure resistance of polycrystals with multiple bulk phases as well as possible tertiary products at grain boundaries (e.g., amorphous films). Realistic geometric renderings of microstructures were generated using the DREAM.3D software package, resulting in Lagrangian meshes that were implemented in numerical simulations. Characterization data provided input to the process, leading to microstructures whose response was validated with tests on the actual material. Modeling of mechanical response of grains and interfaces was undertaken via the phase field approach.

3.3.3 Modeling and Experimental Connections

The multiscale modeling efforts described in Sections 3.3.1 and 3.3.2 connected with experiments for model validation, improved understanding of fundamental mechanisms, guidance for more optimal processing conditions, and targets for microstructural features that improved performance. Experimental backscattered scanning electron microscopy (BSEM)/electron backscattered diffraction (EBSD)/transmission electron microscopy (TEM) images of diamond-SiC interfaces and SiC grain boundaries were used to validate classical atomistic models by directly comparing with globally predicted structures. Atomistic models exploring the elastic-plastic response of the interfaces provided critical insights into their underlying deformation mechanism as they were simultaneously explored

through microcantilever mechanical tests. Interface structures that improve the mechanical response predicted by atomistic models defined targets for experientially engineered boundaries. Initial renderings of mesoscale mechanics models were generated from experimental 3D microstructures for validation by comparing observed and predicted mechanical response and fracture behavior. Microstructure variations predicted to improve the response in the mesoscale mechanics-based models were set as target goals to feed back into experiential processing efforts. A schematic of the intended developmental cycle and interdependencies of modeling and experimentation is shown in Fig. 1.

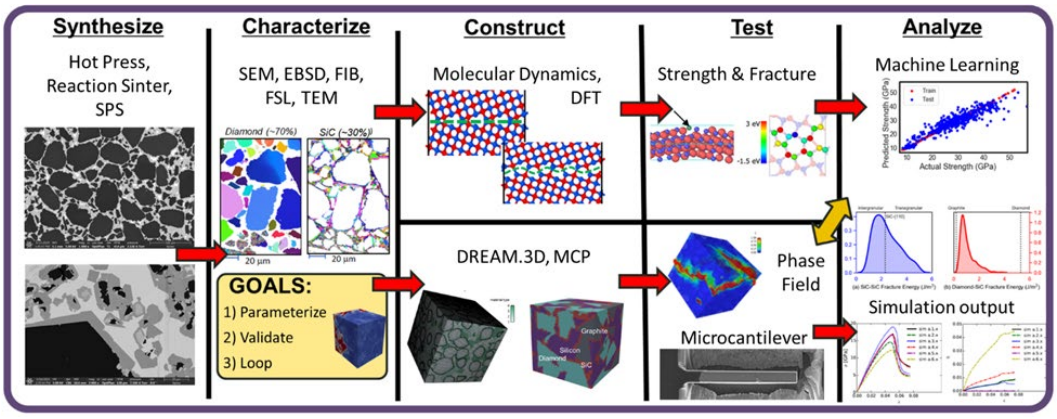

Fig. 1 High-level schematic linking the synthesis, characterization, testing, and evaluation of diamond ceramic composites in this program. Primary goals were to parameterize the microstructure from the atomistic through mesoscale hierarchy using an array of modeling and targeted experimental techniques that validate the outputs and allow iterative developments that improve material properties.

3.4 Terminal Ballistics

Large-scale or full-scale ballistic testing is not feasible for this program and instead focused on sub-scale ballistics testing at extremely fine spatial resolution and shorter time durations. Phase contrast imaging (PCI) experiments using synchrotron-generated X-rays are best suited for such investigations. The Dynamic Compression Sector at the Advanced Photon Source was used to capture time-resolved analysis of dwell and penetration during impact of metallic projectiles into diamond and diamond-SiC composites (8- × 8- × 13-mm specimens). The fundamental insights of these high-rate deformations revealed the governing mechanics of diamond and diamond-based ceramic composites. The impact experiments were compared to baseline experiments on SiC, B_4C, and B_4C/SiC composites to understand the critical stresses and stress states required to cause inelastic deformation, fracture, failure, and onset of penetration in these new novel target materials. Quantitative measurements of dwell as a function of impact stress/velocity, along with penetration velocity measurements and identification of

the spacing orientation and distribution of cracks under terminal ballistic loading, were made.

4. Findings

4.1 Synthesis Results

4.1.1 Hot-Pressing

Hot-pressing is a traditional way to ensure high density for processing powdered ceramic materials in many industries. Two significant challenges arise when hot-pressing diamond powders into a sinterable matrix material. Firstly, the matrix material must densify at temperatures that are not overly detrimental to the diamond, which is a metastable allotrope of carbon and begins to transform to non-diamond carbon at temperatures above 750 °C. Herein, the maximum effective sintering temperatures are 1600 °C based on the kinetics of the conversion.[5] The second critical challenge to overcome is the percolation limit for interparticle contact under densification conditions of the surrounding matrix. Fundamentals of packing theory[15] can provide effective limits for particle arrangements of bimodal and trimodal mixtures. A model of the densification limit was obtained by this investigation[16] and a densification guide was developed for fully dense and partially dense sintered matrix formulations based on the ratio of small-to-large inclusions (Fig. 2). The plot shown in Fig. 3 validates the basic theory for bimodal mixtures of diamond particles that were sintered in a SiB_6 matrix at temperatures up to 1600 °C. The percent total inclusion volume is plotted as a function of the ratio of small to large inclusions, with the final hot-pressed density as a percent of the theoretical density (%TD) shown in the rectangular boxes near the data points.

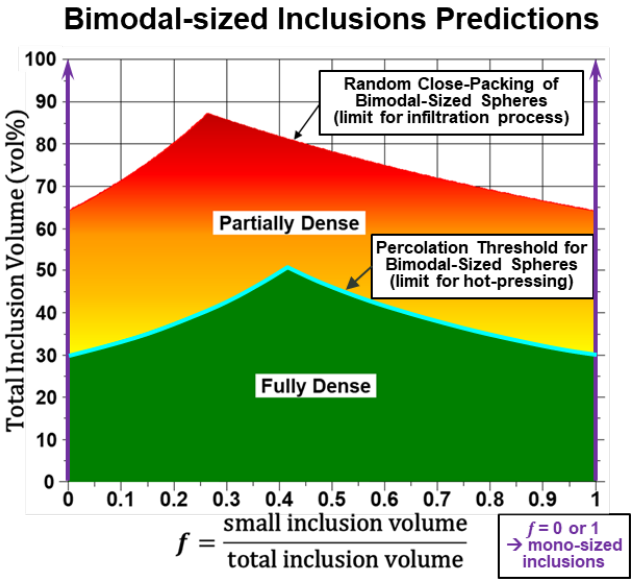

Fig. 2 Theoretical bimodal size inclusions and the predictions of densification regimes for different volume fractions

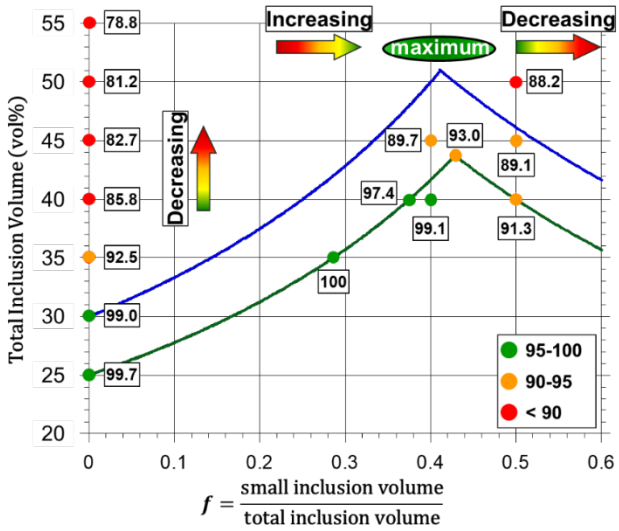

Fig. 3 Experimentally determined densification limits for bimodal inclusions of diamond in a SiB_6 matrix sintered up to 1600 °C. Green, red, and orange circles are experimental data. Theoretical density (%TD) values are shown on the graph near the corresponding circle. Compare with Fig. 2.

4.1.2 Reaction Sintering

The nature of the traditional reaction-bonded diamond-SiC composite synthesis is one of many complexities during densification. A molten silicon phase must infiltrate a tightly packed partially consolidated powder by wetting a multitude of different surfaces. Simultaneously, the wetting infiltrate is reacting with those surfaces, changing the surface wettability, and constricting the open pathways for

infiltrations. Moreover, the wettability and reactivity of the phases is temperature sensitive and the temperature in the bulk sample is in a nonequilibrium state while heat flows from the outer region of the die to the inner as it heats to the peak reaction temperature. Finally, the reaction between molten silicon and carbon is highly exothermic, which further causes locally extreme temperature spikes in the microstructure.[17]

To overcome some limitations with the infiltration approach, the synthesis program investigated the use of a pure powder-based reaction-synthesized diamond-SiC composite by optimizing the distribution and packing of the precursor reactants, including silicon, to achieve higher diamond density than the infiltration approaches. The diamond, graphite, and silicon powders procured for this study (Table 1) were combined to optimize their packing efficiency as shown in Fig. 4. Using an optimized blend of the small, medium, and large silicon powders guided by standard powder packing theory,[15] a pre-reaction green packing density for the diamond, graphite, and silicon mixture of about 79% TD was achieved.

Table 1 Powdered materials used for synthesis

Sample designation	Material	Average particle size (μm)
D181	Diamond	167
MD1020	Diamond	15
Si [L]	Silicon	111
Si [M]	Silicon	44
Si [S]	Silicon	6
1506T	Graphite – spherical	8.5
1520T	Graphite – spherical	17.5
Si97/3	Silicon 97% - Moly 3%	<74

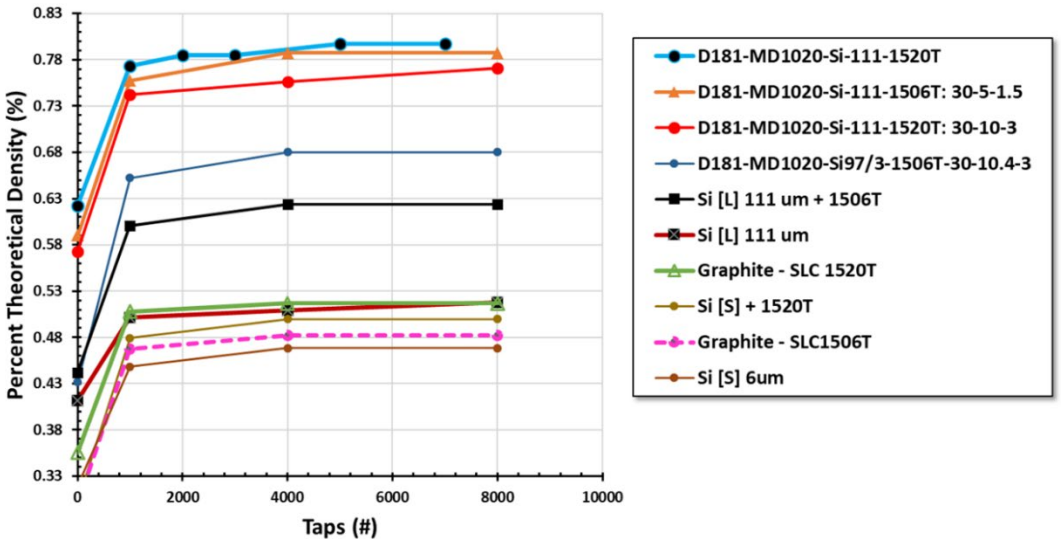

Fig. 4 Packing efficiency from tap densometer measurements on a range of powders used for this investigation (see Table 1). D181-MD 1020-Si-111-1520T, a combination of bimodal diamond, spherical graphite, and trimodal silicon powders, achieved an optimal 79% theoretical dense packing efficiency prior to thermal processing.

The mixtures of dry powder, once optimized for tap density, were combined in a Turbula (Glenn Mills Inc., Clifton, NJ) mixer, weighed, and then pressed in a conventional hot-press die and reaction sintered under moderate pressure (40 MPa). Sintering results for diamond-graphite-silicon powder blends at temperatures between 1500 °C and 1600 °C are shown in Table 2. All the optimization efforts yielded a best density of approximately 2.6 g/cm^3, however, which was too low for testing ballistically owing to large amounts of residual porosity (Fig. 5, left). While volume reductions associated with the formation of SiC were anticipated, the expectation was the volume increasing contributions from converting diamond to non-diamond carbon could compensate, which was not the case for the conditions evaluated.

Table 2 Reaction hot-press sample formulations and synthesis details. Selected samples and their densities demonstrate the limitations of the powder-based reaction synthesis. Sample designations indicate the volume % diamond with the remaining volume fraction comprised of carbon and silicon at ratios of 30:10:3 diamond:silicon:carbon. Excess silicon above the stoichiometric ratio was used to accommodate the conversion of some diamond to non-diamond carbon.

Sample	Hold temp (°C)	Hold time (s)	Load (lb)	Mass (g)	Density (g/cm^3)
82% Dia. + C_{spg}	1600	1800	5500	6.93	2.6
82% Dia. + C_{spg}	1500	3600	5500	6.78	2.6
70% Dia. + C_{spg}	1500	1800	5500	6.18	2.6
70% Dia. + C_{spg}	1500	1800	5500	4.97	2.5
70% Dia. + C_{spg}	1550	1800	5500	2.86	2.7
70% Dia. + C_{spg}	1600	1800	5500	2.89	2.1

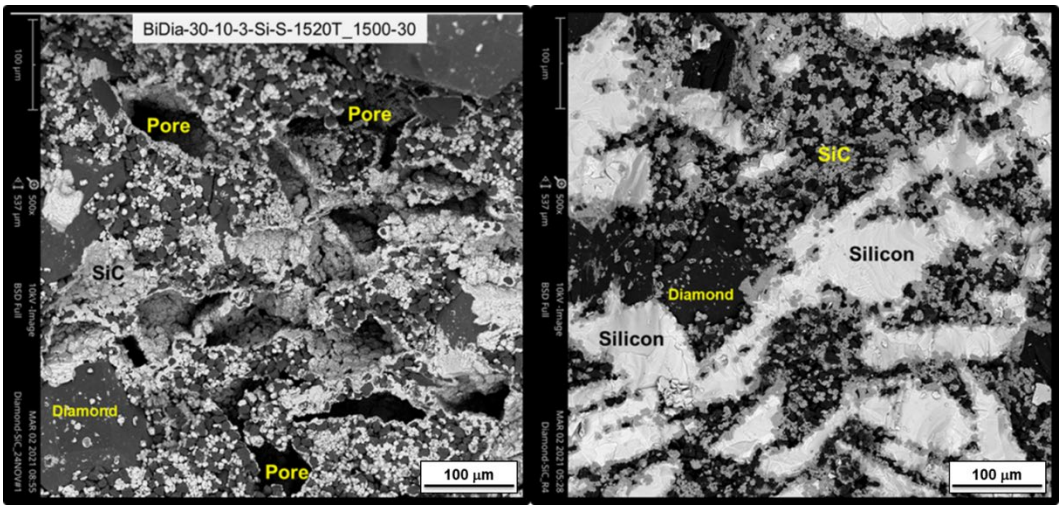

Fig. 5 Reaction sintered diamond-SiC composite. Low density (<2.6 g/cm^3) porous example (left). Silicon reservoir infiltrated sample with increased density of 2.7 g/cm^3 (right). The large porous regions that existed in samples created by the original powder synthesis methodology are shown now to be filled with a silicon phase. The theoretical density of samples made with the silicon reservoir approach increased in density to nearly 90% TD.

An attempt to address the residual porosity, was made by modifying the reaction synthesis process. To the existing process, a reservoir of powdered silicon was added separately into the hot-pressing die, just above the optimized diamond silicon carbon mixture. The applied pressure of the hot-press forced the molten silicon into the open pore space (Fig. 5, right) achieving large gains in theoretical density. The silicon reservoir infiltrated samples produced a high density of 2.7 g/cm^3. TD the of samples made with the silicon reservoir approach increased in density to nearly 90%. The modified approach demonstrated great improvement in density, but overall densities were still too low for ballistic evaluation.

4.1.3 Spark Plasma Sintering (SPS)

SPS is an effective tool to rapidly sinter some materials using bursts of high electrical energy that ultimately enable lower sintering temperatures, shorter hold times, and often increased material properties for sintered bodies compared to conventional methods of densification.[18] Thus, SPS was an attractive method to rapidly densify these materials and potentially avoid some of the pitfalls of normal sintering, especially with the complexities of the reaction and transformation processes.

The first trial was to reduce the sintering temperature of the matrix SiC using known sintering additives such as alumina and boron carbide.[19,20] Figure 6 demonstrates the achievement of full density at temperatures as low as 1725 °C. Formulations of SiC and sintering aid with 40 vol% diamond additions were SPS sintered at temperatures between 1550 and 1725 °C. At temperatures above 1600 °C, the diamond was rapidly transformed to non-diamond carbon and correspondingly, the density of the sintered samples was poor. As the temperature was lowered, the residual diamond content increased, but the temperatures were too low for the matrix to sinter and residual porosity dominated.

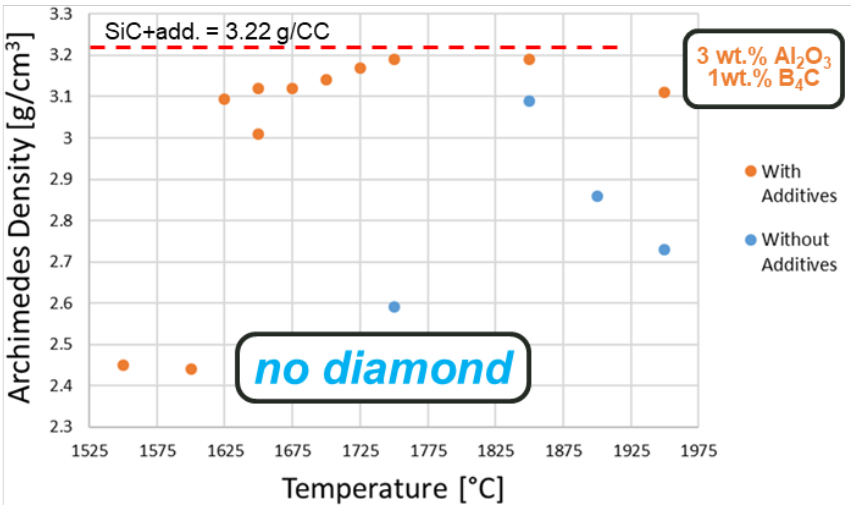

Fig. 6 SPS sintering of UF15 SiC and UF15 SiC plus sintering aids. The results are without diamond additions. Without additives, the pure SiC did not achieve full density. However, the addition of 3 wt% alumina and 1 wt% B_4C enabled essentially full density to be attained as low as 1725 °C.

X-ray Rietveld analysis (Fig. 7) of the diamond and graphitic phases demonstrate the rapid loss of diamond and corresponding increase of graphite phase as the sintering temperature is increased. Furthermore, the peak density of the sintered samples was no higher than 2.9 g/cm^3 measured by Archimedes method, suggesting

significant porosity remained. The phase fractions are detailed in Table 3. As a result, this method was deemed ineffective at producing material worthy of ballistic testing.

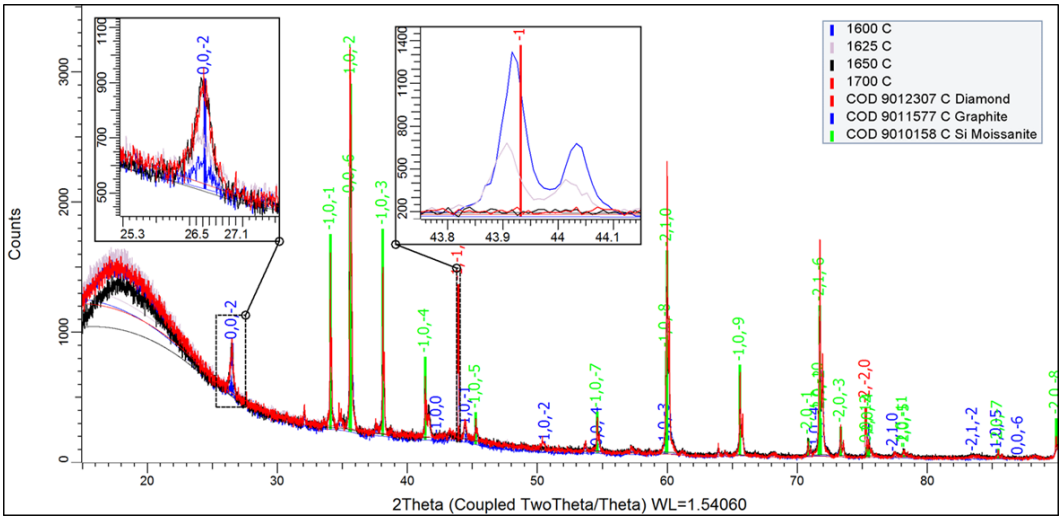

Fig. 7 X-ray 2-theta scans demonstrate the degradation of the diamond volume fraction as sintering temperature increases from 1600 to 1700 °C

Table 3 Phase fractions for SPS diamond composites using a SiC matrix and sintering aids of alumina and B_4C. Graphitic peaks increase correspondingly with the decrease of diamond phase fractions. By 1700 °C, there is very little detectable diamond. Initial starting fraction of diamond was approximately 40 vol%.

Temp (°C)	6H SiC (wt%)	Diamond (wt%)	Graphite (wt%)	ρ_{Th} (Rietveld)	$\rho_{meas.}$ (Archimedes)
1600	69.5	27.1	3.4	3.26	2.59
1625	80.0	14.3	5.7	3.20	2.86
1650	83.9	4.0	15.7	3.19	2.66
1700	86.7	trace	13.3	3.08	2.72

The SPS sintering was also carried out on the optimized diamond, graphite, and powdered silicon mixtures used in the Section 4.1.2 reactive sintering methodology to provide a direct comparison of the consolidation methods. Temperatures between 1450 and 1650 °C were evaluated, and the SPS method was able to achieve increased densities for several formulations up to 2.9 g/cm^3 (Table 4), which exceeded the peak density of 2.7 g/cm^3 using the silicon reservoir reactive hot-pressing method. However, this was still too porous to test ballistically. Effectively, target densities for ballistic testing were estimated to be higher than 3.15 g/cm^3.

Table 4 SPS sintering results for diamond, silicon, and graphite formulations optimized for reaction hot-pressing. Peak density of 2.9 g/cm^3 was achieved and demonstrated a slight improvement over the reactive hot-pressing using the silicon reservoir (2.7 g/cm^3). Densities were still too low for ballistic testing.

Material	Temp (°C)	ρ (g/cm^3)	TD % Reacted	TD % Unreacted
Bi-Dia-+ Si(s) + C(1520T) [Calculated]	1450	3.40	. . .	. . .
Bi-Dia-+ Si(s) + C(1520T) 30:10:3 ratio [Experimental]	1450	2.51	73.9	83.5
	1500	2.87	84.5	95.5
	1550	2.93	86.3	97.5
	1600	2.83	83.3	94.1
	1650	2.5	73.6	83.2

A third and final variation on the SPS densification methodology for the diamond-SiC composites involved the use of a reactive SPS approach (rSPS). The key changes to the process are the incorporation of titanium carbide (TiC)-coated diamond powder blend and the addition of titanium metal powders in combination with the standard Si. Mixtures of Si-Ti-TiC-coated diamond (TCCD) and Si-Ti-uncoated diamond (UD) were sintered via SPS. As the sintering temperature increased, the amount of graphitic content increased for both the TCCD and UD composites. In the case of TCCD, the graphitic content trends consistently upward, whereas for UD, the graphitic content increases but then plateaus at approximately 10 vol%.

The bulk densities for rSPS of SiC-TiC-diamond composites had higher %TD compared to the prior SPS formulations and achieved a peak of 97% TD as shown in Fig. 8. While the TCCD did not necessarily prevent excess graphitization from occurring at all sintering temperatures considered, the TCCD and UD sintered at 1625 °C with approximately the same porosity showed less graphite in the TCCD sample compared with the UD sample. Additionally, the optimal densification (least amount of porosity) occurs at 1625 °C for TCCD and at 1600 °C for UD.

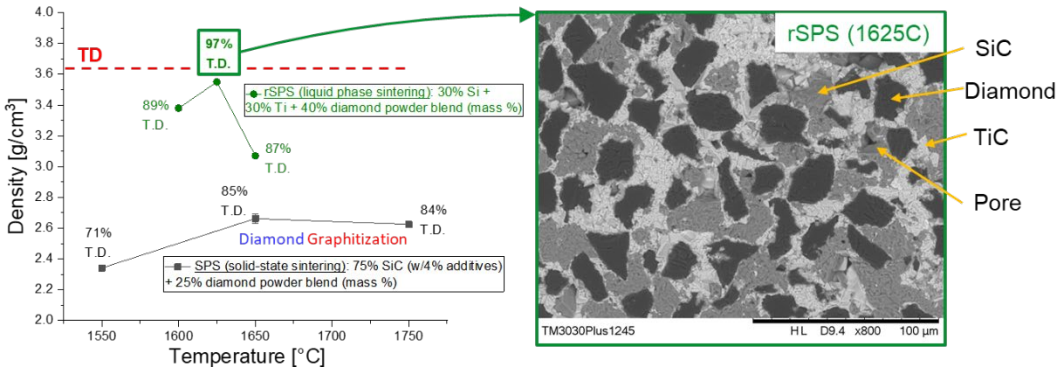

Fig. 8 Densification curves for rSPS of TCCD composites. At 1625 °C a peak density of 97% theoretical and 3.55 g/cm^3 was obtained. Prior to sintering, the composition was 30% Si, 30% Ti, and 40% diamond by mass. For comparison, the solid-state (nonreactive SPS) sintered diamond-SiC materials are shown at the same temperatures with significantly lower theoretical densities.

4.1.4 Graphitization

The graphitization of diamond is a critical transformation that limits the performance of diamond-SiC composites. Specifically, the graphitic phase forms at diamond-SiC interfaces can dramatically reduce the indentation hardness of the diamond composite,[5] where this research showed as little as 25-nm thickness graphitic layer can reduce hardness by approximately 20%. With hardness being a critical property for armor ceramic, such changes could dramatically affect the ballistic performance.

To better understand conditions that lead to detrimental formation of graphite, a simple model based the assumption of spherical diamond particles with a uniform nucleation and growth behavior was created. Validation came from the known activation energy[21] and comparisons with experimental observations in diamond sintered in a SiB_6 matrix as shown in Fig. 9.

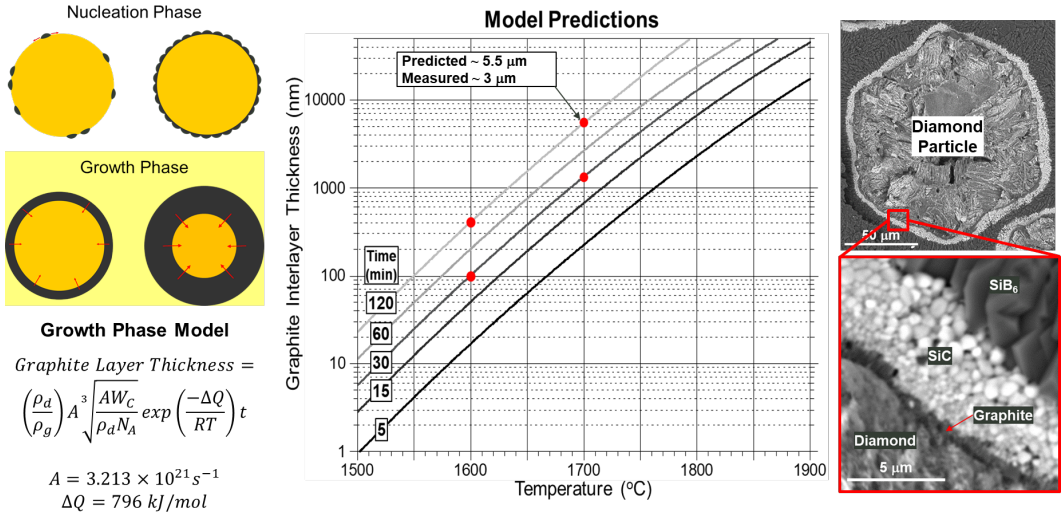

Fig. 9 Simplified nucleation and growth model (left) for the formation of graphitic boundary layers on spherical diamond particles. Model predictions are validated against diamond particles in a SiB_6 matrix (right) and plotted for various time and temperatures (center). Red circles are experimentally determined data and black curves are model predictions. Activation energies for the growth model are from published results.[21]

4.1.5 Bilayer Films

While examining bulk polycrystalline interfaces provides a measure of validation for material development, it is a challenge to control interface chemistry by adapting bulk synthesis conditions. Therefore, to carefully study interfacial phenomena in the diamond/silicon/SiC system, the use of thin films allows for this. Si films of approximately 500-nm thickness were deposited on commercial chemically vapor-deposited (CVD) polycrystalline diamond substrates (Element 6, a De Beers Group, Santa Clara, CA). After deposition, two opposing substrates were sandwiched together such that the exposed surfaces of the deposited silicon were touching. The assembly was placed into a vacuum furnace under light pressure to ensure film contact and heated above the melting point of silicon* to 1550 °C for 30 min. The interaction of silicon with the graphitized diamond interface to form SiC is shown in Fig. 10. Noteworthy in that image is the obvious porosity of the film layer, which underscores further the challenge to achieve full densification that was observed in the bulk samples using the same constitutive phases. At higher magnification (Fig. 11, left) the graphitic boundary between the diamond and SiC is evident. Line traces from electron energy loss spectroscopy (EELS) across the graphitic boundary (Fig. 11, right) show the relative distribution of carbon (violet), silicon (red), and a small amount of oxygen (green). Energy-dispersive X-ray spectroscopy (XEDS) confirmed the bright area in the middle of the interface is

*1414 °C

SiC, the outer region is diamond, and the darker gray region (approximately 100–200 nm in thickness) is graphite.

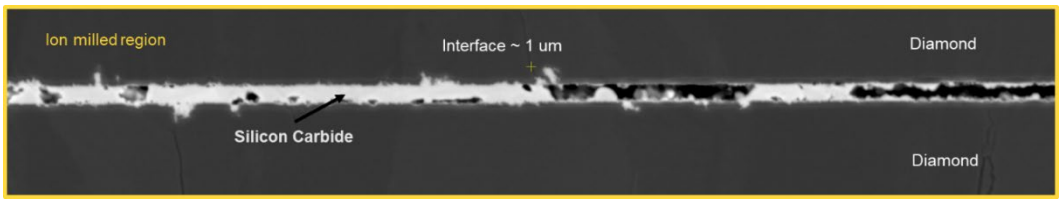

Fig. 10 Polycrystalline diamond substrates with deposited 500-nm films of silicon after heating in vacuum above the melting point of silicon. Image width is approximately 35 µm.

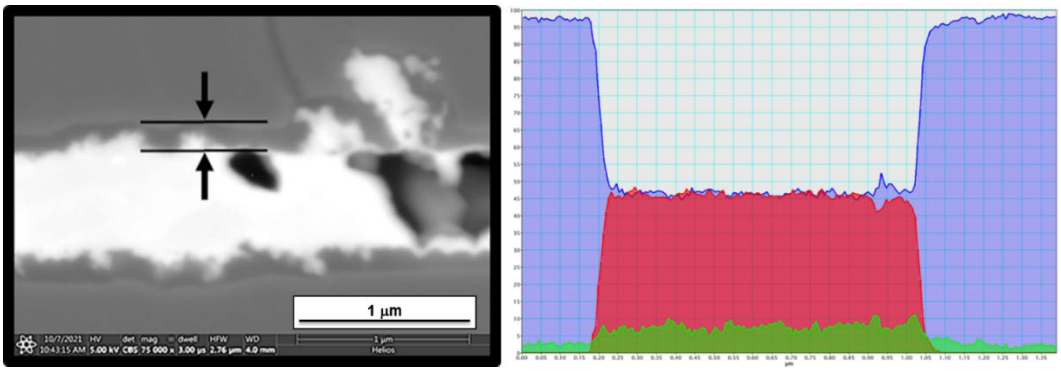

Fig. 11 (Left) Enlarged view of the interfacial region in Fig. 10. (Right) A line trace across the interface shows the relative distribution of carbon (violet), silicon (red), and a small amount of oxygen (green) from EELS. Using XEDS, the bright area in the middle of the interface was confirmed to be SiC, the outer region diamond, and the darker gray region approximately 100–200 nm in thickness is graphite.

4.2 Characterization

4.2.1 SEM/EBSD

To facilitate the development of techniques that eventually validate mesoscale modeling efforts in this program, extensive characterization efforts were applied to commercially available diamond-SiC composites. While characterizing fracture surfaces of diamond-SiC composites offers some guidance, only polished surfaces can be used to accurately determine the key microstructural metrics necessary to inform and validate mesoscale modeling efforts. Diamond-based materials are unable to be polished by conventional means and require special techniques.[22] Polishing of the commercial diamond samples was performed in conjunction with a partner, Applied Diamond Inc. (Wilmington, DE), a company with decades of experience polishing diamond.

A polished sample of diamond composite with approximately 70 vol% diamond is shown in a BSEM image (Fig. 12), where the darkest phase is diamond, intermediate gray is SiC, and bright phase is unreacted silicon. The mesoscale microstructure consists of a wide distribution of diamond sizes, the largest exceeding 50 μm on average. The large diamond grains provide an excellent opportunity to study the interfacial regions of diamond and SiC and as demonstrated in subsequent sections, were characterized extensively.

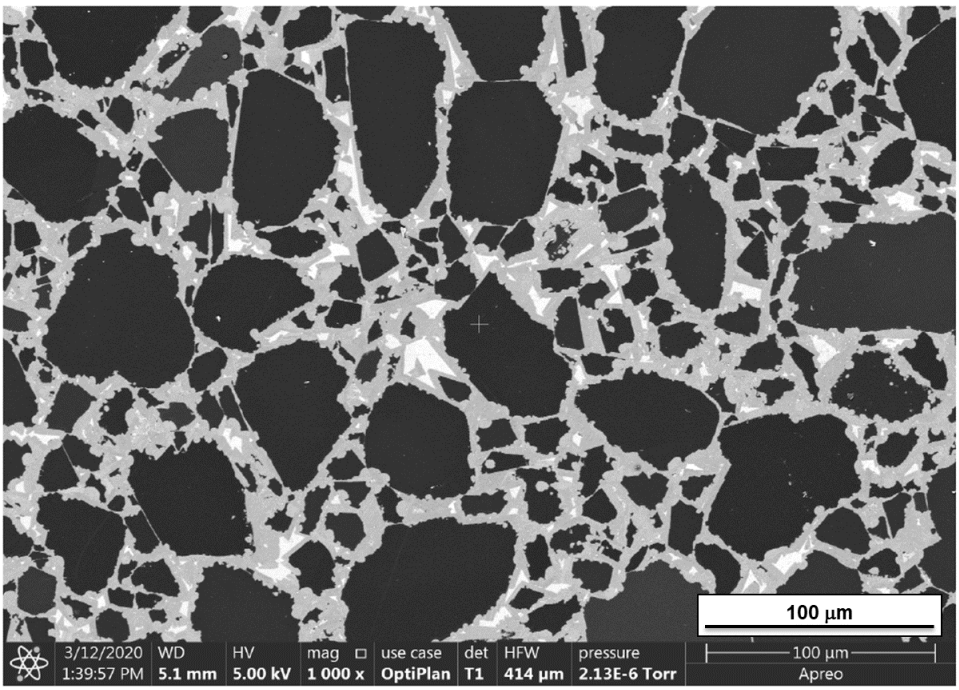

Fig. 12 BSEM image of commercial diamond-SiC composite. Darkest phase is diamond, intermediate gray is SiC, and bright phase is silicon.

To complement the BSEM images, EBSD images were obtained from the polished surfaces. As shown in Fig. 13, orientation mapping of the indexed diamond patterns is on the left for the commercial material with approximately 70 vol% diamond. The right image is the complement to the diamond where only the matrix SiC phase has been indexed (~30 vol%). These data are used to determine the distributions of grain boundary types in the material and inform the mesoscale model development.

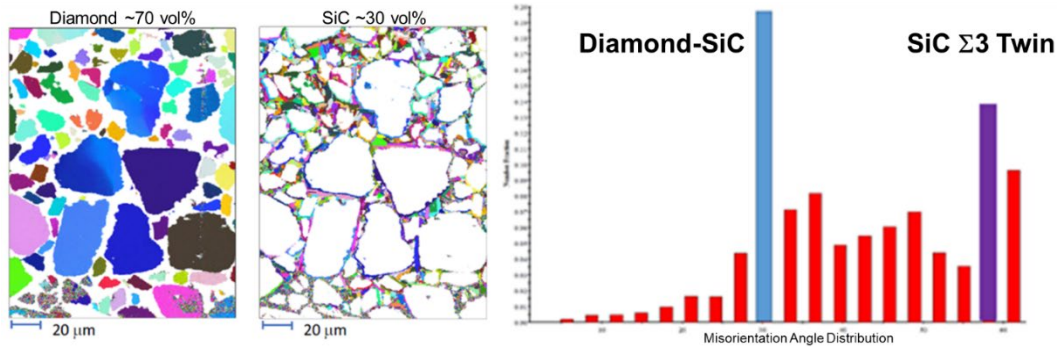

Fig. 13 EBSD image of the commercial diamond-SiC composite. Orientation of the diamond grains is shown for indexed patterns on the left. The center image is the complement to the diamond where the matrix SiC phase has been indexed. These data are used to determine the distributions of grain boundary types, right image, in the material and inform the mesoscale model development. The most prevalent interfaces are diamond bonded to SiC (light blue bar) and the sigma-3 twin boundary in the SiC phase (purple bar).

4.2.2 Bars and Pillars

Mechanical characterization of the bulk diamond composite and targeted interfaces was conducted using a range of advanced characterization techniques. To understand the bulk mechanical response of the diamond-SiC microstructure, novel FSL machining techniques were used to create small-scale fracture bend bars that could be analyzed with a micromechanical testing apparatus.[23] A complementary approach to getting bulk mechanical deformation response under compressive loads is accomplished using micropillars.[24] Finally, targeted microscale fracture, especially at selected interfaces or grain boundary types, may be achieved using a well-established microcantilever bend bar approach, a FIB, and a nanoindenter.[25]

4.2.2.1 Microcantilever Beams

Polished specimens of the commercial diamond-SiC composites were used to create the microcantilever beams used in this study. An example of a typical beam is shown in Fig. 14 where the beam is approximately 30 µm in length and anchored by a diamond phase. In that image, a typical straight boundary interface between the diamond and the SiC is evident.

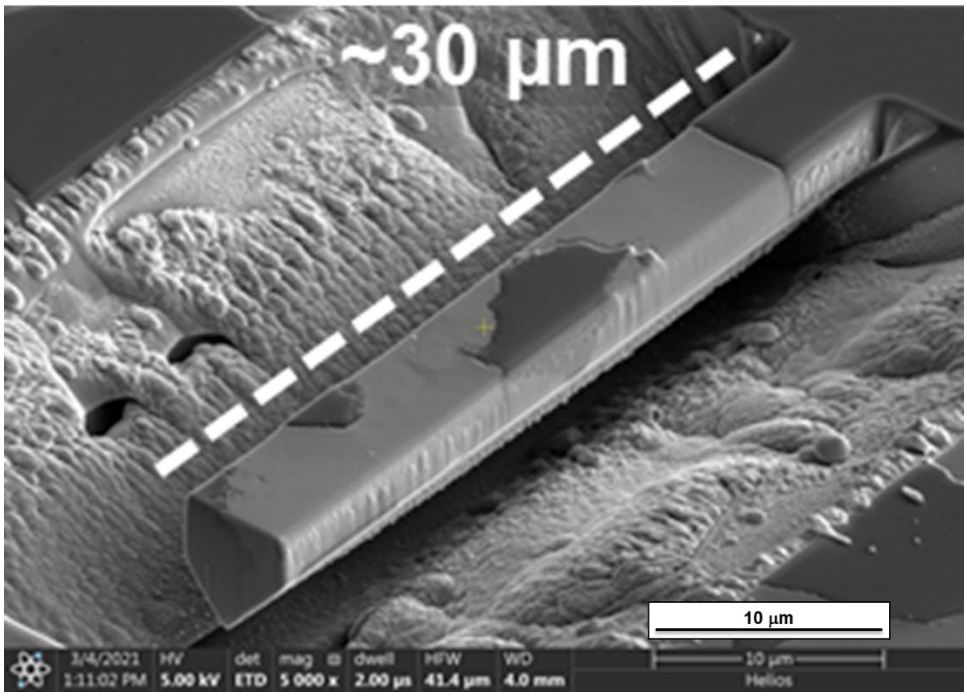

Fig. 14 Microcantilever bend bar in commercial diamond-SiC composite. Bar construction is chosen with the base in a diamond phase. A nanoindenter is used to affect instrumented loading and determine failure.

After collecting a range of BSEM and EBSD images to evaluate the boundary type distribution as shown in Fig. 13, careful evaluation of the boundary interfacial regions revealed two distinct geometries. The first was a straight boundary between the diamond and SiC phase as shown in Fig. 15 (top). The second type of boundary region had prominent curvature as detailed in Fig. 15 (bottom). In those image sequences, the BSEM images are shown on the left and EBSD patterns are shown on the right. The EBSD patterns are not the direct correlations to the BSEM images; hence, they do not match the boundary geometry as shown.

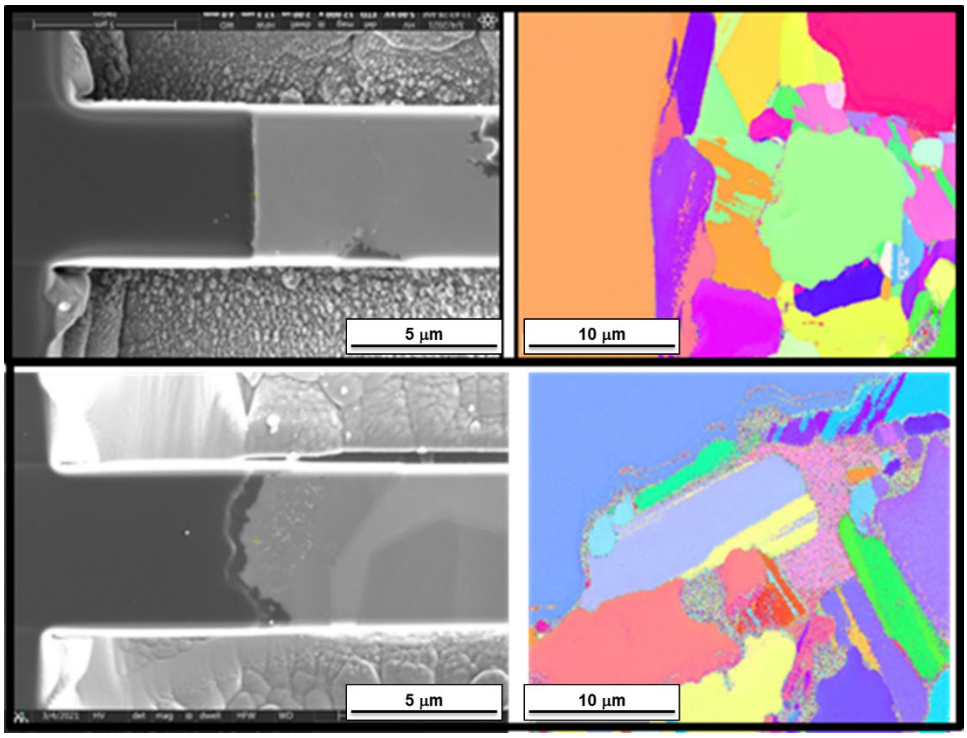

Fig. 15 BSEM (left) and EBSD (right) images of the two main types of diamond SiC interface geometries, nominally straight and curved, that microcantilever bend bars were created for testing interfacial strength

More than a dozen tests were conducted on microcantilever beams to capture the load-displacement failure curves. A majority of the results are shown in Fig. 16 where the dotted line plots are for the curved interfaces and the straight-line plots are for the straight interfaces between the diamond and SiC phases captured by the cantilever beam construction. Two types of diamond-SiC interfaces were observed and tested to failure: curved (C) and straight (S). On average, the load to failure determined from simple beam theory yielded a fracture strength for curved interfaces of 5.51 ± 1.4 GPa and the straight interfaces were 3.82 ± 0.96 GPa as shown in Fig 17.

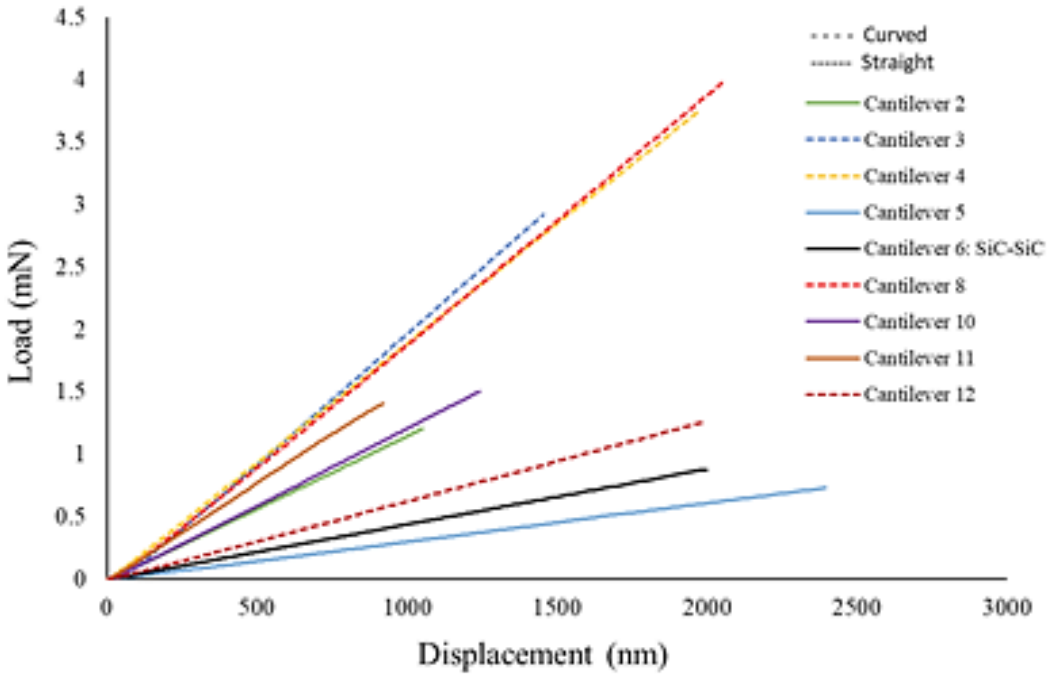

Fig. 16 Load-displacement curves for interfacial microcantilever beams to measure interfacial strength. The dotted line plots are for the curved interfaces and the straight line plots are for the straight interfaces between the diamond and SiC phases. Load is applied until failure using an instrumented nanoindenter.

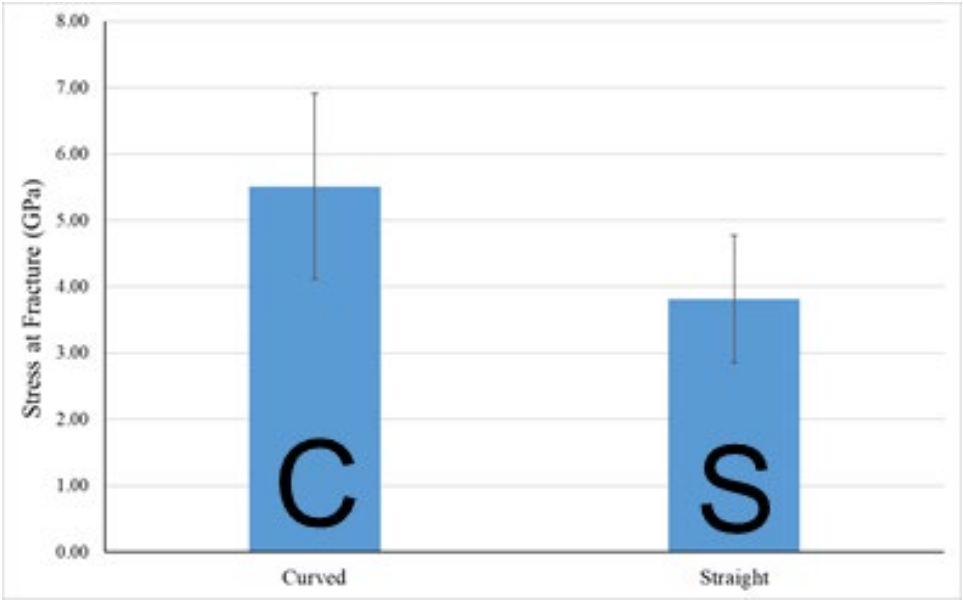

Fig. 17 Isolated strength data for curved (C) and straight (S) boundary types calculated from simple beam theory and the load to failure data. On average, the curved interfaces had a fracture strength of 5.51 ± 1.4 GPa and the straight interfaces were 3.82 ± 0.96 GPa.

While microcantilever beams are effective at targeting interfacial and small-scale features, a better assessment of mesoscale mechanical properties will require a larger beam volume that ultimately averages out more intergranular features. For this, a femtosecond pulsed laser beam was used to machine mesoscale fracture bars of several hundred micrometers in length (Fig. 18). Load was applied with a nanoindenter (Keysight G200), and stress was determined using the moment of inertia of the beam cross section, the applied load, and cantilever length. Fracture tended to initiate in the diamond phase and followed a tortuous path, indicating a high interfacial strength. By measuring the crack size for each flaw an effective toughness can be estimated and compared to known K_{IC} or similar materials. The average cantilever bending strength was measured to be 1296 ± 270 MPa. The individual measurements are detailed in Table 5, with an average fracture toughness measurement determined as 3.17 ± 1.51 MPa-$m^{0.5}$. Also detailed in Table 5 are the peak loads at failure, the calculated fracture stress, and failure initiation point, where D represents failure in the diamond, S is failure in the SiC, and I is at the interface between the two.

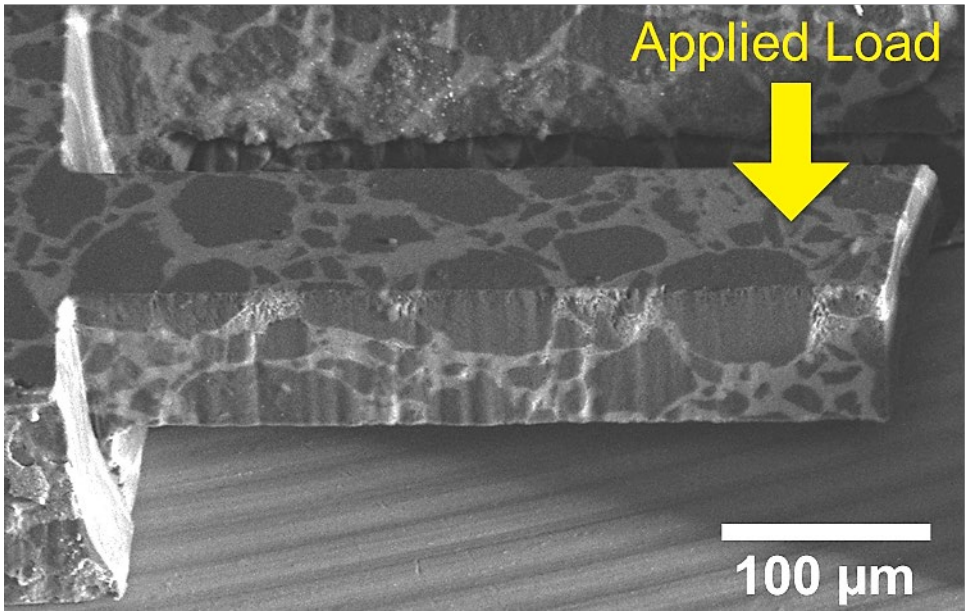

Fig. 18 FSL machined cantilever beam for mesoscale fracture and strength testing

Table 5 FSL machined cantilever bar fracture data. Maximum load, fracture stress, initiation site and stress intensity estimates are tabulated for the 12 tests conducted on a commercial diamond-SiC composite with 70 vol% diamond.

Observation	Max load (mN)	Fracture stress (MPa)	Initiation site	$K_{I,bending}$
1	0.5772	1507	D	4.68
2	0.5993	1709	D	4.29
3	0.4582	1340	I	2.32
4	0.5991	1708	D	6.22
5	0.5044	1456	D	2.33
6	0.4431	1201	S	4.23
7	0.3254	909	D	1.28
8	0.3949	1140	D	1.47
9	0.6071	1289	S	3.42
10	0.6013	1274	D	3.68
11	0.3859	859	S	1.63
12	0.5137	1160	D	2.45
Average	0.5008	1296	. . .	. . .
St. Dev.	0.0987	270	. . .	. . .

Note: D = Diamond; I = Interface; S = silicon carbide.

Observations of the fracture surface indicated a strong diamond-SiC interface based on the transgranular nature of the fracture. Interestingly, fracture was found to initiate more often in diamond grains (67%) compared to within the SiC grains (25%) or interfacially between the two phases (8%). Diamond single crystals have higher fracture energy than SiC single crystals, and diamond-SiC interfaces were found to be weak in the molecular dynamics (MD) studies. The behavior is unexpected, and the present hypothesis suggests inherent defects within the diamond or a grain size effect where the SiC grains tend to be significantly smaller than the diamond grains. Also, interfaces are likely to be misaligned normal to the tensile stress in the polycrystalline materials such that the potential for failure at interfaces is lower. Ultimately, the experimental results suggest that additional refinements to atomistic and phase field models are required to reliably capture the observed behavior.

4.2.2.2 Micropillars

In this study, a micropillar compression test was used to investigate the mechanical behavior of diamond-SiC composites. The micropillars in Fig. 19 were fabricated with a combination of laser and FIB milling to diameters of approximately 25 ± 3 μm by a height of 80 ± 10 μm. Mechanical testing was initiated with a nanoindenter. Pillars fractured after a maximum load was obtained, with an average failure stress, $\sigma = 7.67 \pm 0.69$ GPa. Individual load traces are shown in Fig. 20. The

large scatter in the load-displacement data is likely due to the small size of the micropillar and the large diamond particle size distribution. The strength of the pillar will largely depend on how much diamond phase is captured in the volume.

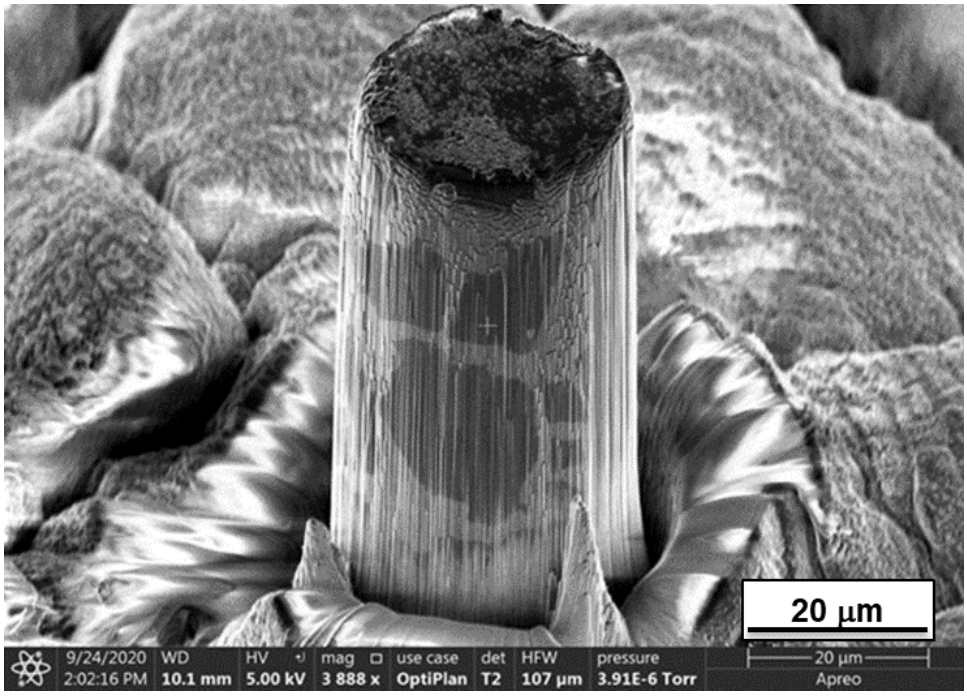

Fig. 19 Micropillar results obtained from commercial diamond-SiC composite materials containing 70 vol% diamond. Pillar formation was achieved with a combination of FIB and FSL to dimensions of approximately 25 ± 3 µm diameter by 80 ± 10 µm height.

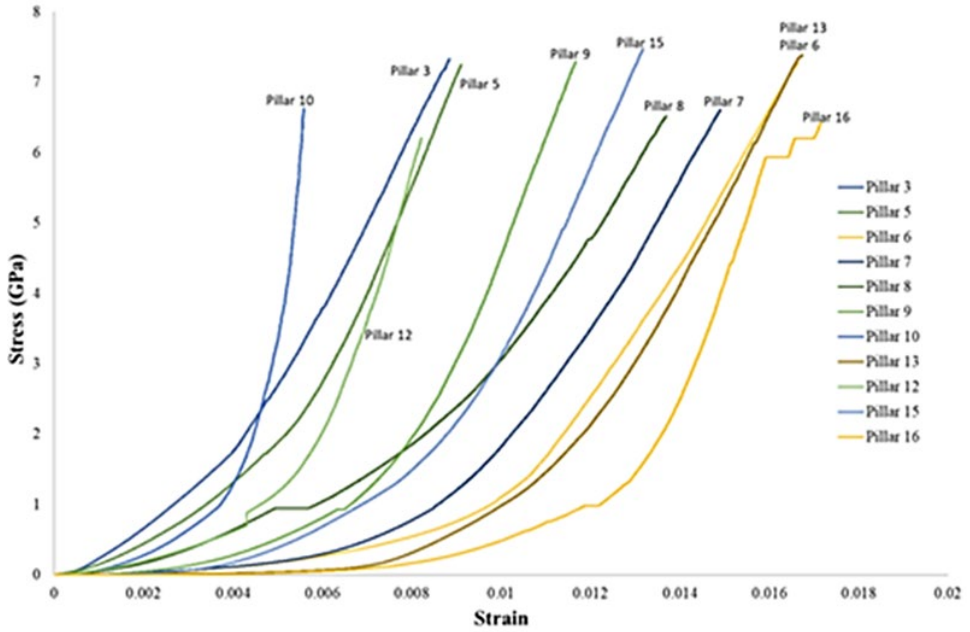

Fig. 20 Load-displacement traces to failure for a dozen micropillar fracture tests

The three mechanical characterization test methodologies all provide viable data to inform the mesoscale phase field models either directly or by focusing atomistic model development that more accurately parameterizes the mesoscale modeling effort. The details of these interdependencies will be discussed in Sections 4.3.2 and 4.3.3.

4.3 Modeling Results

A wide range of sophisticated state-of-the-art modeling efforts were employed to enable more realistic microstructural representation of mesoscale phase field models. Historically, mechanical properties in mesoscale phase field modeling source globally averaged material properties and employed them locally in microstructural models. In this investigation, an attempt to increase the fidelity of the local parameter space within the phase field microstructure was employed by combining results from MD and density functional theory (DFT) atomistic models for grain boundary strength and structure along with validated microstructural characterization as described in the previous sections.

Some key aspects of synthesis and processing variables such as powder packing and microstructural evolution in the diamond-SiC system were also captured using the Large-scale Atomic/Molecular Massively Parallel Simulator (LAMMPS) GRANULAR model and a modified MCP modeling approach.

4.3.1 LAMMPS Particle Packing

The LAMMPS[26,27] is a widely used open-source modeling package. A subdomain of LAMMPS, the GRANULAR package[*], operates like a discrete element modeling code. It uses a "soft sphere" model with Hertzian contact allowing additional terms for tangential, rolling and twisting friction, as well as cohesive forces. GRANULAR was initially used to understand basic powder packing behavior to complement the experimental development and optimization for both the normal hot-pressing and reaction sintering synthesis activities in this program.

Using bimodal particle distributions at several different size ratios, the initial results demonstrated good agreement with published data as demonstrated by the results shown in Fig. 21. The packing relationship for ideal spheres was demonstrated experimentally, using steel shot, by McGeary[28] for size ratios between 3:1 and 19:1 (Fig. 21, left). The LAMMPS code generated results for spherical particles with bimodal ratios between 2:1 and 7:1 (Fig. 21, right). The simulations were limited

[*]https://docs.lammps.org/Packages_details.html#pkg-granular

to a 7:1 ratio owing to the computational time related to the neighbor checking algorithm that is not yet efficient for large size ratios. Nevertheless, the peak packing efficiency for the 7:1 size ratio determined by LAMMPS (81%) is very close to the experimental value of the same ratio (83%).

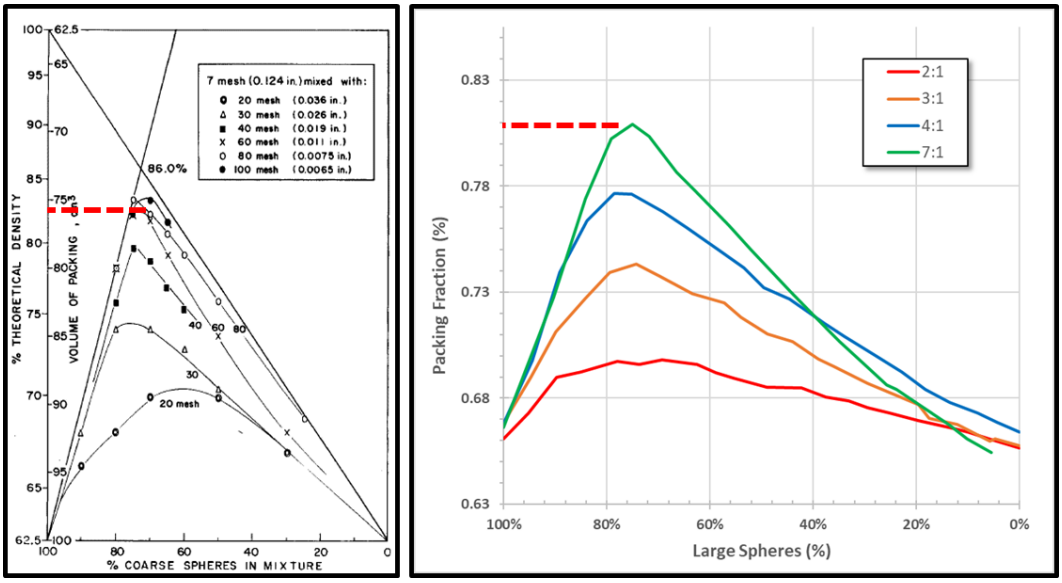

Fig. 21 Bimodal spherical particle packing efficiency for a range of size ratios between 3:1 and 19:1 determined experimentally in McGeary[28] (left) and the LAMMPS GRANULAR particle packing simulations for size ratios 2:1 to 7:1 (right). Peak packing fraction for the 7:1 ratio simulation is in good agreement with experimental results (83% and 81% - dotted red lines).

4.3.2 Grain Boundaries in SiC

To complement the experimental and characterization parts of this diamond-SiC composite investigation and ultimately inform the mesoscale modeling effort, two key grain boundary properties were modeled using atomistic MD. Of primary interest to this investigation were predictions of the grain boundary energy and tensile strength. While predicting the properties of grain boundaries computationally is attractive, it poses significant challenge because of the complex relationships between structural and chemical attributes at both at the atomic and continuum scales. However, compared to the cost and technical difficulty of producing and characterizing individual grain boundaries experimentally,[29] computational methods are preferred because of the amount of data required to build predictive relationships. Herein, crystallographic orientation, structure, and properties of SiC grain boundaries were explored using a combination of high-throughput atomistic techniques and machine-learning methods, which are described in detail elsewhere.[30]

An example of MD output to determine peak tensile strength at a SiC grain boundary is shown in Fig. 22. Based on that approach, the distribution of fracture energies in SiC is evident in the probability distribution shown in Fig. 23 (left) and similarly for the diamond-SiC interface (Fig. 23, right). Notably, the values obtained for the SiC-SiC boundaries fall within the experimentally determined range of fracture energies, 3–7 J/m^2.

These results were incorporated successfully into the phase field mesoscale models to improve the accuracy of the failure predictions as will be described in the next section.

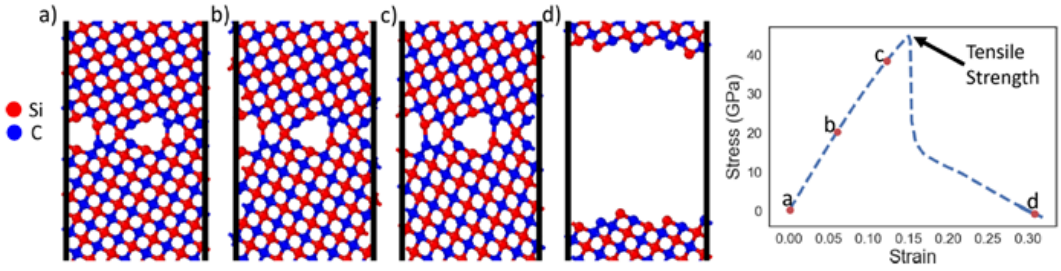

Fig. 22 Example of a tensile simulation used to determine the strength of the grain boundaries considered in this work. Snapshots of the structure of the interface and its corresponding location on the stress−strain curve are shown in a−d.

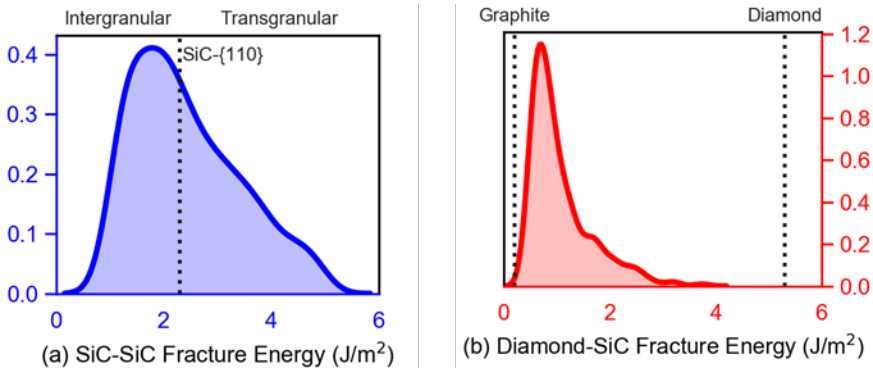

Fig. 23 (a) The probability distribution of fracture energies (J/m^2) at SiC interfaces. (b) A similar plot of fracture energy for the diamond-SiC interfaces. Energies were determined through the strain energy release of the tensile simulations. Results for SiC-SiC were found to agree with the experimentally observed range of fracture energies for polycrystalline SiC of 3−7 J/m^2.

4.3.3 Phase Field Modeling

A new advancement in phase field theory of mesoscale deformation was achieved in diamond-SiC composites by integrating experimental microstructural characterization and MD grain boundary simulations into a micromechanics-based homogenization scheme. Specifically, mesoscale properties, such as distributions of fracture surface energies for different boundary compositions and orientations,

enter a coarse-scale representation of fracture of polycrystalline aggregates in the context of a standard continuum phase field model.[31]

Simulation outputs that were derived by incorporating MD and experimental data from EBSD are new features heretofore unconsidered in prior phase field studies and represent a significant advancement in the art. By using realistically rendered microstructures (i.e., meshes) constructed from diffraction data on real diamond-SiC samples, this study implemented the following:

- Heterogeneous distributions of grain boundary fracture properties obtained from MD simulations, with probed orientation distributions based on EBSD characterization
- Superposition of grain boundary fracture energy distributions obtained from MD with effects of defects, including subscale graphitic inclusions and initial porosity, from elastic homogenization
- Systematic variations of phase content and scale-dependent properties (e.g., bulk microcrystals versus nanocrystalline matrix).

To achieve these novel advancements, the SEM and EBSD statistical feature distributions were importing the into DREAM3D software (v6.5.138, http://dream3d.bluequartz.net), which created a voxelized mesh representation (Fig. 24). Subsequently, the voxel mesh is imported into CUBIT software (v15.6, https://cubit.sandia.gov), where it is transformed to a smoothed hexahedral finite element mesh. Finally, scripting steps are undertaken to assign grain boundary layer regions surrounding larger diamond crystals, and to subdivide matrix material into manageable “grains” among which phases and material properties may vary. The total volume fraction of diamond (70%) is reproduced exactly from the experimental microstructure, with the average equivalent diameter of the 170 large diamond grains in the finite element representation being 20.5 μm.

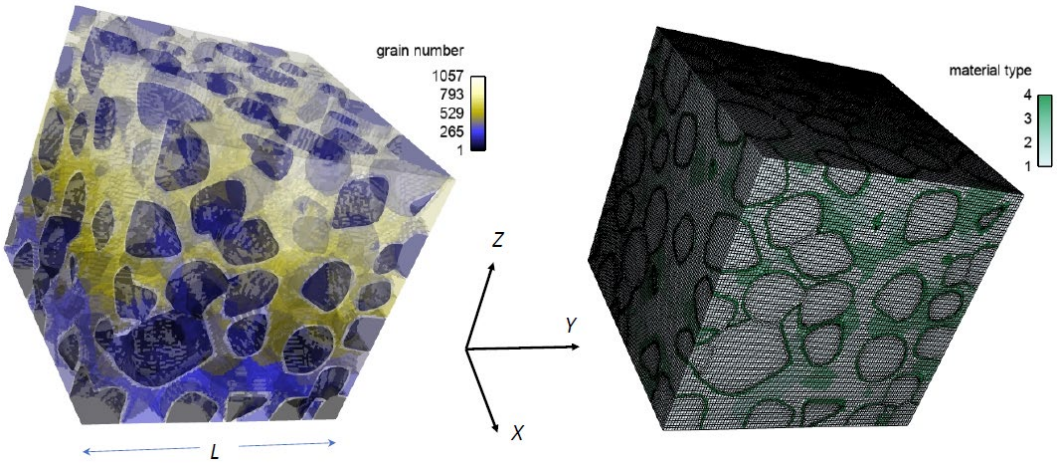

Fig. 24 Reconstructed microstructure based on diamond-SiC characterization data. Grains numbered on left assign a unique number to each discrete grain and to each representative block of SiC matrix. All 170 grain boundary layers are assigned the same "number" (here, 1057; properties that may vary among layers). Mesh with material types on right, where 1 = diamond (anisotropic), 2 = SiC microcrystals (anisotropic), 3 = SiC matrix (isotropic), 4 = grain boundary layer phase (isotropic nanocrystalline; can be SiC, diamond, or graphite).

An example of the evolution of average effective stress, σ, fracture order parameter, ξ, and twinning order parameter, η, are shown in the 3D microstructure for simulation c.6.x (Fig. 25) where compression is in the global X-direction of Fig. 24.[32] Average stress are largest for simulations c.1.g up until peak loading (Fig. 26). Magnitudes are sensitive to initial lattice orientation that controls Schmid factor for elastic driving force for twinning, and therefore loading direction. At larger strains, differences among individual simulations are more pronounced.

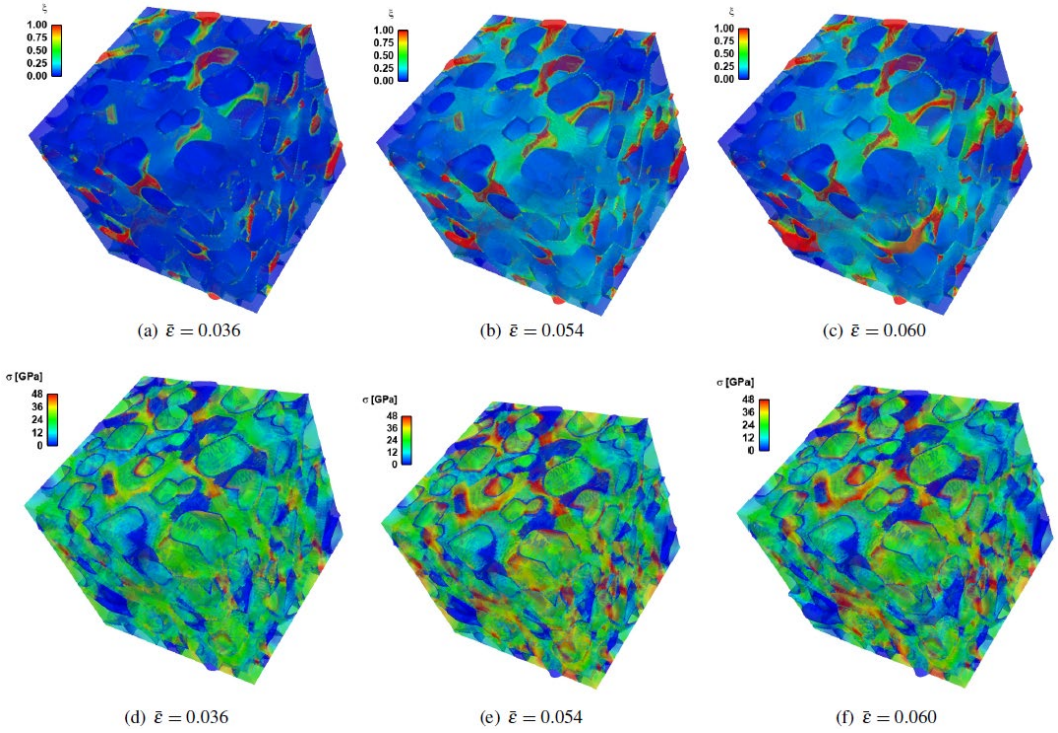

Fig. 25 Stress and fracture order parameter fields for simulation c.6.x (70% diamond, mixed SiC grains and matrix, defective SiC grain boundary layers, MD distributions for intergranular fracture energies, υ_g = 0.4, φ = 0.4, total graphite fraction 5%, total porosity 8%): (a) fracture order parameter ξ, $\bar{\epsilon}$ = 0.036, (b) fracture order parameter ξ, $\bar{\epsilon}$ = 0.054, (c) fracture order parameter ξ, $\bar{\epsilon}$ = 0.060, (d) effective stress σ, $\bar{\epsilon}$ = 0.036, (e) effective stress σ, $\bar{\epsilon}$ = 0.052, (f) effective stress σ, $\bar{\epsilon}$ = 0.060.

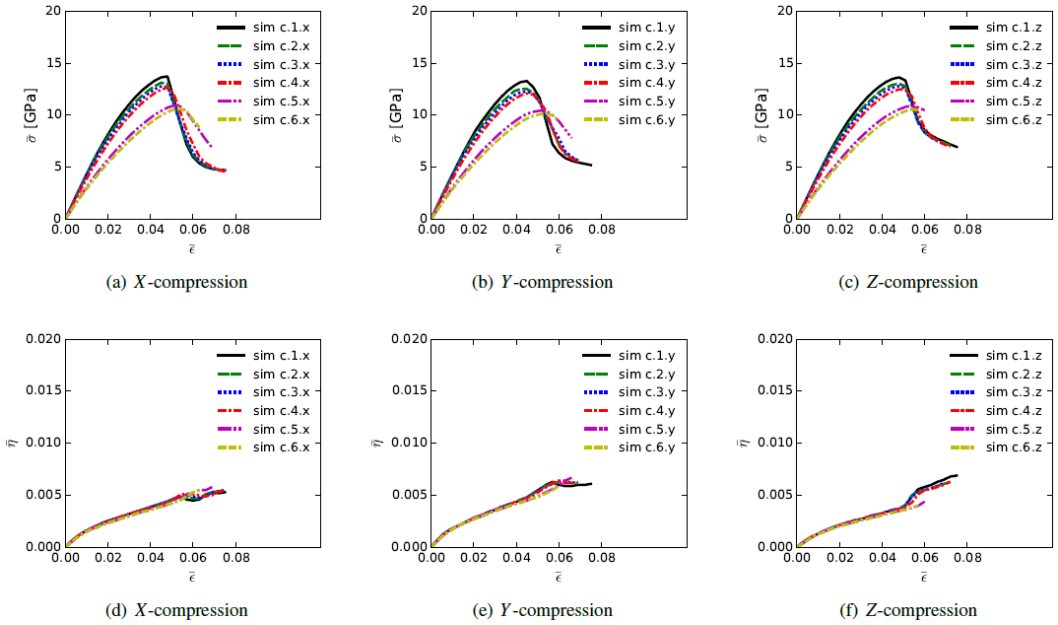

Fig. 26 Effective average (Mises) stress $\bar{\sigma}$, average fracture density $\bar{\zeta}$, and average twin density $\bar{\eta}$ among phase field simulations of Table 4 (refer to Clayton et al.[32]): (a) stress, simulations c.1.x through c.6.x, (b) stress, simulations c.1.y through c.6.y, (c) stress, simulations c.1.z through c.6.z, (d) twinning, simulations c.1.x through c.6.x, (e) twinning, simulations c.1.y through c.6.y, (f) twinning, simulations c.1.z through c.6.z.

Realistic 3D microstructures informed by experimental characterization also allow for more focused parametric studies. As the presence of a grain boundary graphitic phase and porosity are expected to adversely affect the compressive failure of these materials, they were considered parametrically in the simulations. The effects of graphitic phase and void fraction additions were studied parametrically in this same simulation environment. A range of grain sizes, phase content, fracture energy distributions, graphitic layers and inclusions, and voids were incorporated and the effects on strength and fracture were evaluated. Notable findings are summarized as follows:

- Mean fracture energies of diamond-SiC interfaces predicted from MD simulations are substantially lower than those of SiC-SiC interfaces.
- Peak strength and tangent compressive stiffness of the composite increases with increasing diamond fraction when other physical properties are assumed fixed.
- In the absence of porosity or graphite, diamond-SiC boundaries are the weak link in the microstructure; strength and ductility are reduced when the relative fraction of diamond-SiC to SiC-SiC potential fracture sites increases.

- Peak strength and ductility of the composite are substantially reduced when graphitic layers encase large diamond crystals, and these properties are even more compromised when the same fraction of graphite is distributed throughout the whole microstructure.
- Low concentrations of pores and graphite have moderately deleterious effects on strength, but neither significantly reduces the strain at peak load (i.e., these defects do not substantially reduce ductility).
- High global concentrations of pores (8%) cause a much more drastic drop in strength and stiffness than the same global fraction of graphite.
- Twinning occurs in favorably oriented SiC crystals and is sensitive to lattice orientation distribution, but it does not notably alter the overall stress–strain response for the microstructures considered herein.

The implication of these results as feedback to guide future synthesis is one where diamond volume fraction should be maximized when exceptional compressive strength and stiffness is desired, provided that the presence of graphite and voids can be minimized with increasing diamond fraction. In this context, graphite is less harmful to peak compressive strength than voids of the same volume fraction. Although a small amount of porosity may be tolerable, void fractions in excess of an approximate 5% threshold are predicted to degrade severely the overall strength and stiffness of the bulk material.

Furthermore, these findings suggest that the following steps should be undertaken to maximize the average effective strength of diamond-SiC composites, in order of higher to lower priority:

- The volume fraction of diamond should be maximized for a fixed fraction of grain boundary phase of nanocrystalline SiC (here 20%), without increasing porosity or graphite content.
- The volume fractions of graphite and voids in the grain boundary phase should be minimized.
- If a median fraction of voids or graphite is unavoidable, distributions of these defects should be uniform rather than random to minimize extreme weak links in the microstructure.
- Inelastic dilatation (e.g., associated with jagged fracture surfaces) increases peak compressive stress and pressure-dependency of strength.

- At maximum bulk diamond fraction, deformation twinning in the grain boundary phase (3C-SiC) can increase both ductility and peak strength, since it replaces fracture as an inelastic accommodation mode.
- At lower diamond volume fractions, deformation twinning in bulk SiC crystals increases ductility, but peak strength and stiffness are both compromised as the material flows more plastic-like.

Notable limitations to be revisited in future work include the elastic homogenization model for isotropic effective grain boundary properties that omits locally complex defect structure (e.g., pore clusters, thin graphite layers versus inclusions), the empirical relations (motivated by observations on other ceramics) assumed for effects of pores on effective surface energy of the grain boundary regions, and the idealized synthetic polyhedral grain and phase morphologies used in finite element simulations.

4.3.4 Monte Carlo Potts Modeling

The purpose of this work is to develop a mesoscale model to predict microstructure evolution in Si/SiC/C systems. To achieve this study in three dimensions, as topology of particles is important, a first-of-its-kind modeling approach had to be developed. Starting with the fundamental MCP model used to study grain growth and recrystallization, modifications now allow consideration of arbitrary numbers of phases within the Si/SiC/C system relevant to this investigation. In contrast to historical MCP codes, which only update based on "local" configurations, this model studies critical physical phenomena (formation of SiC through increasingly thick diffusion layers) via long-range behavior using a newly developed search scheme for large 3D volumes of simulated material. By subdividing space hierarchically, the code allows for fast searching of nearest reaction sites between Si and C through SiC regions enabling the breakthrough findings. Additionally, the model implicitly includes diffusion-limiting effects of the formation of an intermediate phase layer, using distance between parent phases. By selecting sites of a given phase and proposing a new "reaction" step to them (Si or C to SiC), it identifies partner voxels to react simultaneously. The energy change of this step includes the energy change that occurs at all considered voxels. Lastly, to model the growth of SiC grains more accurately within the microstructure, a machine-learned model for grain boundary energy is used to determine neighboring SiC voxels with different orientations. Specifically, the quarternion angle between the voxels is used to produce inputs into a Gaussian process regression model, trained on grain boundary energies determined by MD, to use more realistic energies at only a small computational cost (Fig. 27).

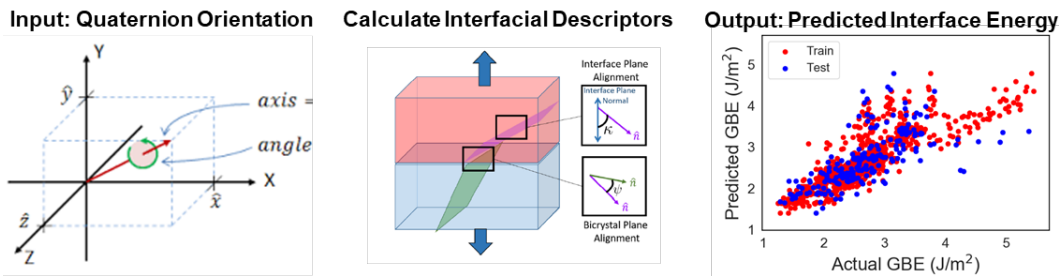

Fig. 27 Dynamically evolved microstructure model improved by interface energies obtained from machine-learning-optimized grain orientations

One critical factor in the example system of Si/SiC/C is the formation of any graphitic phase. Herein, graphitization is handled on a boundary-by-boundary basis, separate from the bulk allotrope conversion process and prior to the reaction phase growth. Graphitization affects grain boundaries and mobility, though the model only handles graphite growing on the SiC/C interfaces, which then affects phase change rates in the rest of the model. Because the exact impact is unknown, a kinetics factor k is varied, which is a term that slows reaction/boundary motion rates as graphite layer thickness increases. Conservation laws mean that there is long-range correlation in reaction rates across this new phase; for example, every atom of C that contributes to SiC also needs a Si partner. To overcome an anticipated slower operation for the code with this complexity, active learning, a semi-supervised machine-learning approach that can be used to select query points in a sequential experimental process, is used to improve computational efficiency.

The effect of particle size against reaction rate on model output, as well as reaction behavior on sharp, faceted particles, was tested using an even mix of Si and C with tetrahedral particle aggregates. Such aggregates were created by placing tetrahedral objects of fixed size inside the volume, with some allowed overlap as shown in Fig. 28 t_0.

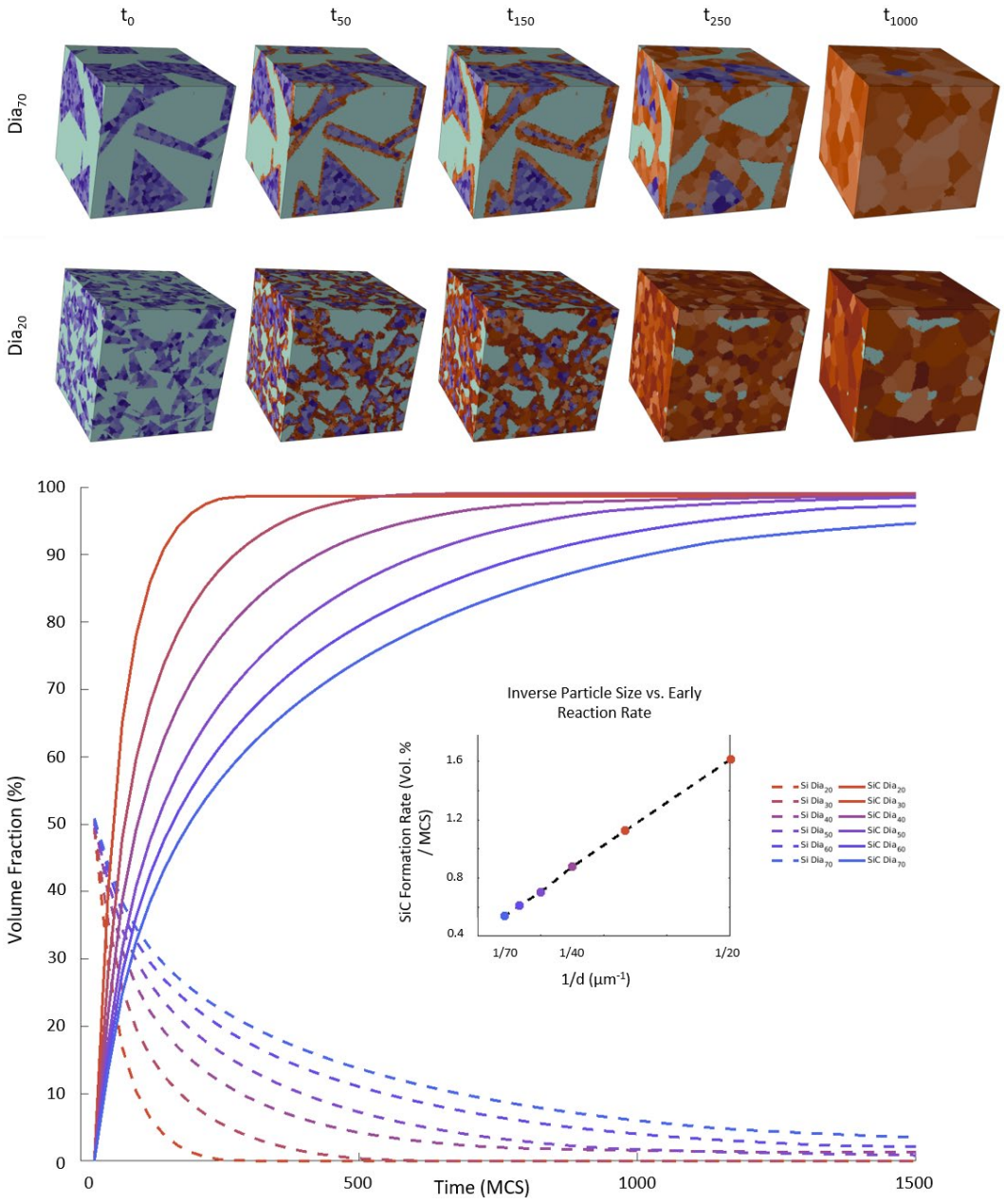

Fig. 28 Phase fraction evolution of pointed diamond particle systems as function of particle size, with select microstructure examples at various times for the 20- and 70-µm particle size cases. Polycrystalline silicon is shown purple, diamond is shown light cyan, and SiC is depicted as orange. Graph inset shows reaction rate vs. inverse particle size during the first 25 time steps.

Because particle size critically affects reaction pathway, smaller particles with higher surface area to volume ratios should react commensurately faster. An inverse size effect was demonstrated with the early reaction rate (e.g., as seen in the inset plot of Fig. 28). The simulation outputs illustrate further the impact of size effects, using tetrahedral-based particle aggregates using an even mix of Si and C, where

near-complete reactions were anticipated and ultimately observed (Fig. 28 t_{1000}). The particle's shape was also found to accelerate the rate of reaction. Sharp corners and edges contributed to the reaction of the particles compared with smooth, spherical particles or flat planar surfaces, until the inner diamond core becomes somewhat rounded.

A powerful advantage of the MCP simulations was demonstrated in a combination with the previously described LAMMPS GRANULAR outputs. The spherical packing of realistic distributions of diamond particles from GRANULAR, validated with experimental powder packing data, can serve as a realistic starting point for the MCP microstructural phase evolution and ultimately link macroscopic processing conditions to simulated microstructural evolution, which can also be validated experimentally. A simple example is shown for both monosized (r = 25 μm) and bimodal sized (r = 25 μm and r = 50 μm) diamond particles in Fig. 29. The diamond particle packing is shown as light cyan spheres. By incorporating polycrystalline silicon in the open space of the packing model, the conversion of diamond to graphite and subsequent reaction with silicon as temperature is elevated, can be simulated. Early stage MCP output demonstrates the transition of diamond into SiC and ultimate conversion of the matrix silicon (purple) into SiC (orange). These results demonstrate the connection between macroscale particle processing details to microstructural evolution in the simulation space.

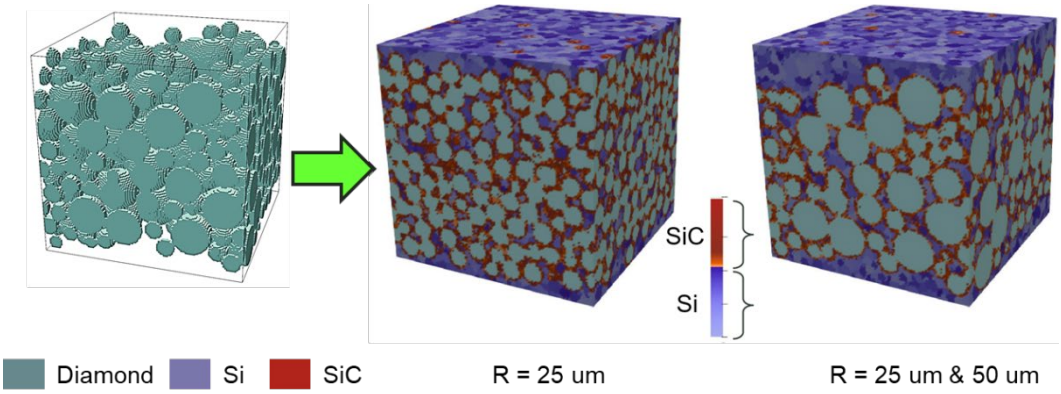

Fig. 29 LAMPS GRANULAR spherical particle packing with relevant physics for a bimodal distribution of diamond particles (left) (monosized diamond not shown). Early stage modified MCP simulations for the diamond spheres (light cyan) embedded in polycrystalline silicon (purple) and their conversion to SiC (orange). The simulation results demonstrate the connection between macroscale particle processing details and microstructural evolution in the simulation space.

An added benefit of the MCP simulation output was the ability to establish a critical link between the MCP output domain and the mesoscale input domain. An interpreter code was developed that allows the simulated microstructural data to flow from the MCP through DREAM3D and be rendered visually and meshed appropriately to be read into the phase field code as demonstrated in Fig. 30.

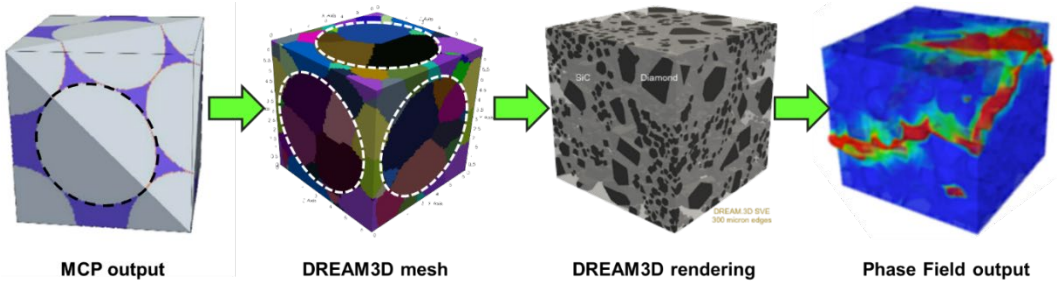

Fig. 30 Data transfer pathway for MCP output to be integrated into mesoscale phase field models through DREAM3D. The MCP output is captured into DREAM3D, where it can be rendered and/or interpolated into the appropriate mesh scheme to implement in the phase field environment. This data stream represents a critical link to establish a feedback loop in the processing and evolution of microstructure and the ultimate performance at the mesoscale.

In summary, this developed a new Monte Carlo approach to study the formation of reaction-bonded stoichiometric phases concurrently with other microstructure evolution processes. This approach is computationally efficient enough to conduct even large simulations on an end-user computing system and is made parallelizable for use on high-performance systems such as the DoD HPC. In conjunction with powder-packing models, this approach becomes a powerful link in engineering microstructure from systems that use reaction bonding or similar processes. Though calibrated for SiC in this work as a demonstration, this approach can be readily generalized to several other multicomponent systems with stoichiometric phases.

4.4 Subscale Ballistics

Subscale ballistic experiments this program relied on an advanced high-speed PCI technique implemented at the Argonne National Laboratory's Advanced Photon Source (APS) within the Dynamic Compression Sector (DCS) X-ray beamline.

PCI offers the ability to conduct high-precision dynamic impact experiments with submicrosecond temporal resolution to characterize the damage response during impact. The imaging scintillator is not placed immediately behind the sample, but at a known distance so the radiation refracted by the sample can interfere with the unchanged beam. This configuration produces stronger contrast, outlining the surfaces and structural boundaries of the sample (edge enhancement) compared with conventional radiography. PCI relies on gradients in the phase of transmitted

X-rays where features like crack surfaces induce a steep gradient, significantly enhancing contrast.

The small-scale terminal ballistic test setup used at DCS for this study is shown in Fig. 31, where the projectiles were made of oxygen-free high thermal conductivity (OFHC) copper and impacted targets that were adhesively bonded on top of a tungsten or carbide backer.

The ballistic results for polycrystalline CVD diamond and the commercial 70 vol% diamond-SiC used in this investigation both demonstrated exceptional performance relative to the baseline legacy armor ceramics, B_4C and SiC. The specific ballistic results are contained in a limited distribution report[33] with high-speed X-ray images, depth of penetration, penetration transition velocities, and Tate target resistance values and will not be shown here.

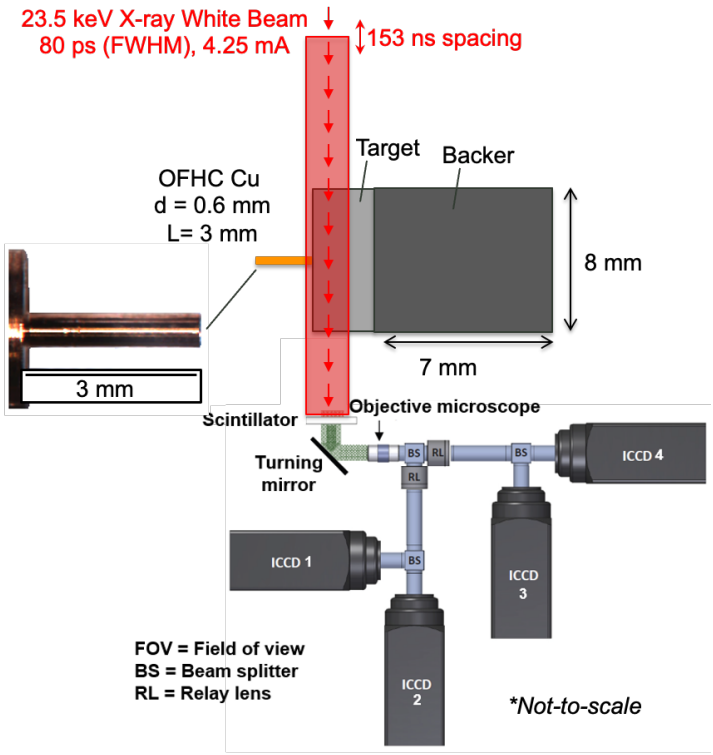

Fig. 31 Sample setup and testing configuration for subscale ballistic testing at DCS beamline, Argonne National Laboratory APS. Copper penetrator of L/d = 5 impinges on the strike-face with the 24-keV white X-ray beams transversely penetrating the sample and captured by the scintillators. Field of view during impact is ~2.5 mm and image capture is about one frame per 153 ns.

4.5 Major Partners

University of Connecticut: CRADA 14-020-003/C Atkinson (DEVCOM ARL supported: ORAU W911NF-21-2-0058)

University of Delaware/Sandia National Laboratories: CRADA-10-051-J005

University of North Texas: DoD Joint Faculty Appointment – T Scharf

Fraunhoffer IKTS: W911NF2020115/50:50 split CCDC Atlantic Office

PEO Solider: MIPR Applied Diamond Inc. – W911QX-19-P-0102

Commercial Vendor (II-VI M-Cubed): informational exchange/sample material

DEVCOM Soldier Center: testing of commercial tiles

5. Recommendations

Based on the findings of this program, continued development of the mesoscale fracture models is warranted. The program's connection and improvement at the mesoscale with atomistic calculations and experimental observations require additional links to the macroscale and continuum models. Existing DEVCOM ARL programs in continuum mechanics models should be adapted to interface with the phase field codes from this study.

In parallel to the linking of the phase field modeling to macro and continuum scale modeling is the 3D MCP study that established critical processing variable links to the evolved microstructures. The digitization and transformation of the MCP-evolved microstructures into the mesoscale phase field modeling environment, by way of the DREAM3D interface, is a new and highly exploitable modeling capability that has only just begun to show its eventual promise.

Following from the aforementioned modeling breakthrough using MCP and phase field, further refinements and links into the processing space are feasible via the LAMMPS GRANULAR particle code. As many metal and ceramic synthesis methods are powder-based, the GRANULAR code has the requisite physics to capture basic particle-particle interactions of powder flow and packing. The distribution of powder packing can form the starting or nucleation points for microstructure evolution in the MCP code and as demonstrated previously, be validated through characterization, experimental testing, and physical property evaluations at the mesoscale with phase field modeling. The fidelity of each of these modeling pathways improves with continued development, validation, and interoperability.

The reaction synthesis methods should be focused on modifying the traditional liquid silicon infiltration work that was the mainstay of material synthesis for diamond-SiC composites. Focus should be on leveraging the packing optimization and LAMMPS GRANULAR code to investigate routes to optimize the infiltration efficiency, minimize unreacted silicon, and control final microstructure to improve the scaled-up ballistic testing with actual threats.

6. Payoff/Army Impact

- This investigation is the largest and most comprehensive experimental, characterization, and modeling development activity to study SiC diamond composites. Furthermore, the findings of the program are generalizable to other materials and contribute substantially to the DEVCOM ARL's ability to investigate in a comprehensive manner the understanding and optimization of materials to meet a variety of Army mission requirements.
- Knowledge about the diamond-SiC material system is exploitable beyond armor and has significant performance enhancements as a thermal management material, especially where high strength, wear, and corrosion resistance are a concern.
- This knowledge will enable DEVCOM ARL researchers to manipulate Army-relevant materials at the microstructural level to exhibit superior mechanical properties at the system level. This will facilitate the development of robust materials for Army protection/lethality systems.
- This program established a link between simulated microstructural evolution derived from a modified MCP approach and translated that output in 3D to a functional input for the micromechanical mesoscale phase field modeling environment. This capability allows for more direct and rapid investigations of the link between processing variables and relevant performance for Army materials.

7. Program Publications/Patents

- Clayton JD, Guziewski M, Ligda JP, Leavy RB, Knap J. A multi-scale approach for phase field modeling of ultra-hard ceramic composites. Materials. 2021;14(6):1408.

- Guziewski M, Montes de Oca Zapiain D, Dingreville R, Coleman SP. Microscopic and macroscopic characterization of grain boundary energy and strength in silicon carbide via machine-learning techniques. ACS Applied Materials & Interfaces. 2021;13(2):3311-3324.
- Clayton JD, Zorn JA, Leavy RB, Guziewski MC, Knap J. Phase field modeling of diamond-silicon carbide ceramic composites with tertiary grain boundary phases. International Journal of Fracture. 2021;1-38.
- Tavenner JP, Weinberger CR, Coleman SP, Tucker GJ. Probing fundamental deformation mechanisms and trends during decohesion across random high angle grain boundaries. Computational Materials Science. 2021;186:110063.
- Guziewski M, Banadaki AD, Patala S, Coleman SP. Application of Monte Carlo techniques to grain boundary structure optimization in silicon and silicon-carbide. Computational Materials Science. 2020;182:109771.
- Montes de Oca Zapiain D, Guziewski M, Coleman SP, Dingreville R. Characterizing the tensile strength of metastable grain boundaries in silicon carbide using machine learning. The Journal of Physical Chemistry C. 2020;124(45):24809-24821.
- Guziewski M, Coleman SP, Weinberger CR. Atomistic investigation into interfacial effects on the plastic response and deformation mechanisms of the pearlitic microstructure. Acta Materialia. 2019;180:287-300.
- Clayton JD, Leavy RB, Knap J. Phase field modeling of heterogeneous microcrystalline ceramics. International Journal of Solids and Structures. 2019;166:183-196.
- Magagnosc DJ, Schuster BE. Fracture strength of hot-pressed silicon carbide at the microscale. Materials Science and Engineering: A. 2019;765:138297.
- Clayton JD. Computational modeling of dual-phase ceramics with Finsler-geometric phase field mechanics. Computer Modeling in Engineering & Sciences. 2019;120(2):333-350.
- Atkinson Cassidy M, Guziewski Matthew, Coleman Shawn P, Nayak Sanjeev K, Alpay S Pamir. First principles analysis of impurities in silicon carbide grain boundaries. Acta Materialia. In Press.

- Mallick DD, Leong FT, Tonge AL, Schuster BE. Time-resolved and post-mortem observations of dynamic fragmentation in boron carbide. International Journal of Impact Engineering. 2021 Sep. In review

8. Program Technical Reports

- Dunn Jennifer, et al. Density functional theory study of Σ9 {122} grain boundaries in silicon and silicon carbide-3C. Army Research Laboratory (US); 2020. Report No.: ARL-TR-9057.
- Atkinson Cassidy, et al. Density functional theory study of the impact of impurities in silicon carbide bulk and grain boundaries. Army Research Laboratory (US); 2019. Report No. ARL-TR-8836.
- LaSalvia Jerry, et al. Development and assessment of uniaxial densification limit models for particulate bodies with mono- and bimodal-sized rigid spherical inclusions. Army Research Laboratory (US); 2020. Report No. ARL-TR-9116.
- Trujillo Dennis. Machine learning for predicting properties of silicon carbide grain boundaries. Army Research Laboratory (US); 2019. Report No. ARL-TN-0981.
- Parker Thomas. Plasma-enhanced chemical vapor deposition on diamond powders to enable next-generation hard armor. DEVCOM Army Research Laboratory; 2021. Report No. ARL-TR-9299.
- Ligda Jonathan, et al. Sample preparation methods for diamond-silicon carbide microstructure analysis. Army Research Laboratory (US); 2020. Report No. ARL-TR-8887.
- DiGiovanni Anthony, et al. High-speed synchrotron X-ray study of sub-scale ballistic impact and penetration of thick CVD diamond substrates. DEVCOM Army Research Laboratory; Forthcoming 2022.

9. Program Invited Presentations

- LaSalvia J, et al. Effects of diamond content and modality on the densification of diamond particulate ceramic composites by hot-pressing. TMS. 2020.

10. Program Presentations/Posters

- Guziewski M, et al. Bridging the nano- to meso-scales for microstructural modeling of ceramic composites. ICACC. 2021.
- LaSalvia J, et al. Effect of hot-pressing parameters on diamond graphitization and hardness of diamond particulate ceramic composites. TMS. 2021.
- LaSalvia J, et al. Theoretical limit for the content of rigid spherical inclusions in a hot-pressed ceramic. ICACC. 2021.
- Guziewski M, et al. Multi-scale modeling of hierarchical microstructure in ceramic composites. TMS. 2021.
- Guziewski M, et al. Characterizing the energetics and structural configurations of silicon carbide grain boundaries using high-throughput atomistic techniques. TMS. 2020.
- Dunn J, et al. DFT modeling of effect of processing additives on grain boundary stability and cleavage behavior in SiC diamond composites. MEDE. 2020.
- Ligda J, et al. Influence of three-dimensional microstructure on the impact response of advanced ceramics. MS&T. 2020.
- Mallick D, et al. Laser-driven shock of protection ceramics. MEDE. 2020.
- DiGiovanni A, et al. Reaction sintered silicon carbon diamond composites via optimized particle distributions. ICACC. 2020.
- Guziewski M, et al. Understanding the energetics and structure of interfaces in silicon carbide-diamond composites using high-throughput atomistic simulations and machine learning. ICACC. 2020.
- LaSalvia J, et al. Densification of monomodal & bimodal diamond particulate - sib6 composites by conventional hot-pressing. ICACC. 2020.
- Guziewski M, et al. Workflow for high-throughput atomistic models of silicon-carbide grain boundaries. ICACC. 2019.
- LaSalvia J, et al. Densification of mono-sized diamond particulate - ceramic composites by conventional hot-pressing. ICACC. 2019.
- LaSalvia J, et al. Densification of particulate bodies containing rigid mono-sized spherical inclusions by hot-pressing. MEDE. 2019.

- Clayton J, et al. Phase field theory and analysis of fracture and dynamic transformation kinetics in polycrystalline ceramics and ceramic composites. MACH. 2021. Poster
- 1st Place Award POSTER COMPETITION (44th International Conference on Advanced Ceramics and Composites, Daytona Beach, January 2019)
    - Atkinson C, et al. DFT study of the impact of defects in SiC bulk and grain boundaries. ICACC. 2019.
- 2nd Place Award POSTER COMPETITION (44th International Conference on Advanced Ceramics and Composites, Daytona Beach, January 2019)
    - LaSalvia J, DiGiovanni A, Behler K. Diamond-ceramic composites by reactive hot-pressing.

11. References

1. Vargas-Gonzalez L, Speyer R, Campbell J. Flexural strength, fracture toughness, and hardness of silicon carbide and boron carbide armor ceramics. International Journal of Applied Ceramic Technology. May 2010;7:643–651.

2. LaSalvia JC, Campbell J, Swab JJ, McCauley JW. Beyond hardness: ceramics and ceramic-based composites for protection. JOM. 2010;62:16–23.

3. LaSalvia JC, McCauley JW. Inelastic deformation mechanisms and damage in structural ceramics subjected to high-velocity impact. Int J Appl Ceram Technol. 2010;7:595–605.

4. Kidalov S, Shakhov F. Thermal conductivity of diamond composites. Materials (Basel). 2009;2:2467–2495.

5. Herrmann M, Matthey B, Höhn S, Kinski I, Rafaja D, Michaelis A. Diamond-ceramics composites-New materials for a wide range of challenging applications. J Eur Ceram Soc. 2012;32:1915–1923.

6. Kennedy P, Parkinson K, inventors; United Kingdom Atomic Energy, assignee. Reaction bonded silicon carbide artefacts. United States patent US 4,536,449. 1985 Aug 20.

7. Kennedy P, North B, inventors; United Kingdom Atomic Energy, assignee. Silicon carbide bodies and their production. United States patent US 4,299,631. 1981 Nov 10.

8. Brown WG, inventor; Coors Porcelain Company, assignee. Method for manufacturing silicon carbide bodies. United States patent US 4,154,787. 1979 May 15.

9. Salamone S, Neill R, Aghajanian M. Si/SiC and diamond composites: microstructure-mechanical properties correlation. In: Singh D, Salem J, Mathur S, Ohji T, editors. Mechanical properties and performance of engineering ceramics and composites V: ceramic engineering and science proceedings, volume 31. The American Ceramic Society. 2010;97–106. doi:10.1002/9780470944127.ch11.

10. Gordeev SK, Zhukov SG, Danchukova LV, Ekström T, inventors; Ambler Technologies, Inc., assignee. Method of manufacturing a diamond composite and a composite produced by same. United States patent US 6,447,852. 2002 Sep 10.

11. Gordeev SK, Zhukov SG, Danchukova LV, Ekström T. No low-pressure fabrication of diamond–SiC–Si composites. Inorg Mater. 2001;37:579–583.

12. Matthey B, Höhn S, Wolfrum AK, Mühle U, Motylenko M, Rafaja D, Michaelis A, Herrmann M. Microstructural investigation of diamond-SiC composites produced by pressureless silicon infiltration. J Eur Ceram Soc. 2017;37:1917–1928.

13. Zhao Y, Qian J, Daemen LL, Pantea C, Zhang J, Voronin GA, Zerda TW. Enhancement of fracture toughness in nanostructured diamond-SiC composites. Appl Phys Lett. 2004;84:1356–1358.

14. Lundberg P, Renström R, Lundberg B. Impact of metallic projectiles on ceramic targets: transition between interface defeat and penetration. Int J Impact Eng. 2000;24:259–275.

15. German, RM. Particle packing characteristics. Metal Powder Industries Federation; 1989.

16. LaSalvia JC, DiGiovanni AA, Guziewski MC. Development and assessment of uniaxial densification limit models for particulate bodies with mono and bimodal sized rigid spherical inclusions. CCDC Army Research Laboratory; 2020. Report No.: ARL-TR-9116.

17. Hofbauer PJ, Rädlein E, Raether F. Fundamental mechanisms with reactive infiltration of silicon melt into carbon capillaries. Advanced Engineering Materials. 2019;21(8):1900184.

18. Munir ZA, Anselmi-Tamburini U, Ohyanagi M. The effect of electric field and pressure on the synthesis and consolidation of materials: A review of the spark plasma sintering method. Journal of Materials Science. 2006;41(3):763–777.

19. Zhou Y, Tanaka H, Otani S, Bando Y. Low-temperature pressureless sintering of alpha-SiC with Al4C3-B4C-C additions. Journal of the American Ceramic Society. 1999;82(8):1959–1964.

20. Gubernat A, Stobierski L, Łabaj P. Microstructure and mechanical properties of silicon carbide pressureless sintered with oxide additives. Journal of the European Ceramic Society. 2007;27(2-3):781–789.

21. Davies G, Evans T. Graphitization of diamond at zero pressure and at a high pressure. Proceedings of the Royal Society of London. A. Mathematical and Physical Sciences. 1972;328(1574):413–427.

22. Malshe AP, Park BS, Brown WD, Naseem HA. A review of techniques for polishing and planarizing chemically vapor-deposited (CVD) diamond films and substrates. Diamond and Related Materials. 1999;8(7):1198–1213.

23. Magagnosc DJ, Schuster BE. Development of femtosecond laser based microscale fracture methods. In Mechanics of Biological Systems & Micro- and Nanomechanics. Springer, Cham. 2019;4:15–16.

24. Shin C, Jin HH, Kim WJ, Park JY. Mechanical properties and deformation of cubic silicon carbide micropillars in compression at room temperature. Journal of the American Ceramic Society. 2012;95(9):2944–2950.

25. Ast J, Matthey B, Herre P, Höhn S, Herrmann M, Christiansen SH. Micro-cantilever testing of diamond-silicon carbide interfaces in silicon carbide bonded diamond materials produced by reactive silicon infiltration. Open Ceramics. 2021;8:100176.

26. Plimpton S. Fast parallel algorithms for short-range molecular dynamics. Journal of Computational Physics. 1995;117(1):1–19.

27. Thompson AP, Aktulga HM, Berger R, Bolintineanu DS, Brown WM, Crozier PS, in't Veld PJ, Kohlmeyer A, Moore SG, Nguyen TD, Shan R, et al. LAMMPS-a flexible simulation tool for particle-based materials modeling at the atomic, meso, and continuum scales. Computer Physics Communications. 2022;271:108171.

28. McGeary R. Mechanical packing of spherical particles. Journal of the American Ceramic Society. 1961;44(10):513–522.

29. Trahanovsky ME. Bicrystal-array fabrication. University of California, Berkeley; 2012.

30. Guziewski M, Montes de Oca Zapiain D, Dingreville R, Coleman SP. Microscopic and macroscopic characterization of grain boundary energy and strength in silicon carbide via machine-learning techniques. ACS Applied Materials & Interfaces. 2021;13(2):3311–3324.

31. Clayton J. Nonlinear fracture mechanics. In: Altenbach H, Ochsner A, editors. Encyclopedia of continuum mechanics; Springer; 2018.

32. Clayton JD, Guziewski M, Ligda JP, Leavy RB, Knap J. A multi-scale approach for phase field modeling of ultra-hard ceramic composites. Materials. 2021;14(6):1408.

33. DiGiovanni A, Jannotti P, Schuster B, Lorenzo N, Ligda J, Sietins J, Sun J, and Brennan R. High-speed synchrotron X-ray study of sub-scale ballistic impact and penetration of thick CVD diamond substrates. DEVCOM Army Research Laboratory; 2022 Forthcoming.

List of Symbols, Abbreviations, and Acronyms

2D	two-dimensional
3D	three-dimensional
AEM	analytical electron microscopy
APS	Advanced Photon Source
ARL	Army Research Laboratory
BSEM	backscattered scanning electron microscopy
CRADA	Cooperative Research and Development Agreement
CVD	chemically vapor-deposited
DCS	Dynamic Compression Sector
DEVCOM	US Army Combat Capabilities Development Command
DFT	density functional theory
DOD	Department of Defense
DOF	degrees of freedom
EBSD	electron backscatter diffraction
FIB	focused ion beam
FSL	femtosecond laser
HPC	high-performance computing
LAMMPS	Large-scale Atomic/Molecular Massively Parallel Simulator
LC-FIB	coupled focused ion beam
MCP	Monte Carlo Potts
MD	molecular dynamics
MIPR	Military Interdepartmental Purchase Request
NIST	National Institute of Standards and Technology
OFHC	oxygen-free high thermal conductivity
ORAU	Oak Ridge Associated Universities
PCI	phase contrast imaging

rSPS	reactive SPS
SEM	scanning electron microscopy
SPS	spark plasma sintering
STEM	scanning transmission electron microscopy
TCCD	Si-Ti-TiC-coated diamond
TD	theoretical density
TEM	transmission electron microscopy
UD	Si-Ti-uncoated diamond
XRD	X-ray diffraction

1 (PDF) DEFENSE TECHNICAL INFORMATION CTR DTIC OCA

1 (PDF) DEVCOM ARL
FCDD RLD DCI
TECH LIB

1 (PDF) DA HQ
DASA(R&T)

9 (PDF) USARMY AFC
L BROUSSEAU
J REGO
A LINZ
K WADE
S BRADY
J REGO
T KELLY
E JOSEPH
B SESSLER

2 (PDF) DEVCOM HQ
FCDD ST
C SAMMS
M HUBBARD

3 (PDF) SURVICE ENG
B SCHUSTER
M KORNECKI
V RAJU

91 (PDF) DEVCOM ARL
FCDD RLC
C BEDELL
B SADLER
B PIEKARSKI
H EVERITT
FCDD RLC CA
L KAPLAN
FCDD RLC ES
G VIDEEN
S HILL
Y PAN
FCDD RLC I
B MACCALL
FCDD RLC N
BM RIVERA
A SWAMI
FCDD RLD
P BAKER
A KOTT
S SILTON
FCDD RLW B
J LASALVIA
FCDD RLD D
T ROSENBERGER
FCDD RLD E
KS FOSTER
FCDD RLD F
K KAPPRA
FCDD RLD FR
M TSCHOPP
FCDD RLD FS
S COLEMAN
FCDD RLW M
R BRENNAN
FCDD RLW MB
J LIGDA
D MAGAGNOSC
B POWERS
FCDD RLW MC
S WALCK
FCDD RLW ME
A DIGIOVANNI
M GUZIEWSKI
S HIRSCH
M IVILL
W SHOULDERS
FCDD RLW MF
P GOINS
FCDD RLD SM
L BLUM
FCDD RLH
J CHEN
PJ FRANASZCZUK
C LANE
K MCDOWELL
FCDD RLH B
JJ SUMNER
FCDD RLH F
JR GASTON
FCDD RLH T
D STRATIS-CULLUM
FCDD RLL
T KINES
FCDD RLL D
J S ADAMS
FCDD RLL DP
J MCCLURE
FCDD RLR
B HALPERN
S LEE
D STEPP
FCDD RLR E
RA MANTZ
C VARANASI
FCDD RLR EL
JX QIU
MD ULRICH
FCDD RLR EN

RA ANTHENIEN JR
FCDD RLR IC
MA FIELDS
SP IYER
FCDD RLR IM
JD MYERS
FCDD RLR IN
XN WANG
FCDD RLR
P REYNOLDS
FCDD RLR P
LL TROYER
FCDD RLR PC
D POREE
FCDD RLR PL
MK STRAND
FCDD RLS
J ALEXANDER
M GOVONI
M WRABACK
FCDD RLS C
M REED
FCDD RLS CC
S BEDAIR
FCDD RLS CE
TR JOW
K XU
FCDD RLS CL
M DUBINSKIY
FCDD RLS E
RD DELROSARIO
FCDD RLS ED
K JONES
FCDD RLS EA
A ZAGHLOUL
FCDD RLS ER
M NEUPANE
T IVANOV
FCDD RLS S
WL BENARD
FCDD RLS SO
W ZHOU
FCDD RLW
S KARNA
JF NEWILL
AM RAWLETT
SE SCHOENFELD
J ZABINSKI
FCDD RLW B
R BECKER
FCDD RLW M
ES CHIN
FCDD RLW S
V CHAMPAGNE
AL WEST
FCDD RLW T
RZ FRANCART
FCDD RLW TC
JD CLAYTON
R LEAVY
T SCHARF
FCDD RLW TF
D MALLICK
FCDD RLW W
TV SHEPPARD
FCDD RLW WA
B RICE
R PESCE-RODRIGUEZ
FCDD RLW M
A HALL